

POLITECNICO DI TORINO

Master Degree in Aerospace Engineering

Master Degree Thesis

Failure Analysis of Cross-Ply Laminates



Supervisor

prof. Matteo Filippi

Candidate

Francesco Calleri

Tutor

PhD. Marianna Maiarú
University of Massachusetts Lowell

Academic Year 2019/2020

Alla mia famiglia
Alla nonna Luisa

Abstract

This thesis focuses on understanding the failure mechanism of fiber glass reinforced laminates loaded in transverse tension. Fiber-reinforced composites are widely used in engineering applications including aerospace, automotive and wind energy for their high specific properties. Cross-ply laminates are analyzed using Continuum Damage Mechanics (CDM) methods to predict crack formation, propagation and strength of in 'in-situ' 90-ply. The Crackband method proposed by Bazant and Oh, is implemented within the Finite Element Method (FEM) to preserve mesh objectivity in the failure simulations. Analysis are carried out in Abaqus/Standard and Abaqus/EXPLICIT supplemented by user-written subroutines. First, a homogenized model is built to determine the converged size of a Representative Volume Element (RVE) according to the shear lag theory. Then, a detailed model of the RVE that accounts for fibers in the in-situ ply is generated. The zero ply are modeled as homogenized material using Glass Fiber Reinforced Epoxy properties. The influence of the transverse ply thickness on the failure mechanism of the composite is investigated keeping the thickness of the zero plies constant to $d=0.5$ mm while the 90-ply thickness ranges from 0.1 mm (thin ply) to 2 mm (thick ply). Different failure criteria have been studied including the maximum principal stress and the Hashin's Failure Criteria. Results are discussed in term of onset of the microcracking with respect to the in-situ ply thickness.

Acknowledgements

First of all, I would like to thank Professor Marianna Maiarù for the opportunity she gave me and for the great experience at UMass Lowell. Her passion and enthusiasm for the research were a big motivation for the period I spent in the United States and will be a big encouragement for the future.

I would also like to thank the WindSTAR Industrial Advisory Board (IAB) for funding of this project. I would also like to thank WindSTAR IAB members Paul Ubrich, Nathan Bruno, Mirna Robles (Hexion Inc.), Steve Nolet, Amir Salimini(TPI Composites), Bruce Burton, Mark Chouinard (Huntsman Corporation) for their technical support. This material is based upon work supported by the National Science Foundation under Grant Number IIP-1362022 (Collaborative Research: I/UCRC for Wind Energy, Science, Technology and Research). Any opinions, findings and conclusions or recommendations expressed in this material are those of the author and do not necessarily reflect the views of National Science Foundation.

In addition, I would like to express my gratitude to Professor Matteo Filippi, my supervisor at Politecnico di Torino, for his guidance and support from Italy.

Contents

List of Figures	5
1 Introduction	9
1.1 Advanced Composite Materials	9
1.1.1 Composite materials - Matrices	11
1.1.2 Composite materials - Fibers	11
1.2 Applications of advanced composite materials	16
1.2.1 Aerospace applications	16
1.2.2 Wind energy applications	18
1.3 Motivation	18
2 Failure of composites Laminates	27
2.1 Shear Lag Theory	27
2.2 Failure in composites	31
2.3 Delamination	37
3 Finite Element Method Model	41
3.1 Representative Volume Element	41
3.2 Modelling strategy	42
3.3 Damage model	43
3.3.1 Hashin's Failure Criteria	43
3.3.2 CrackBand Model	44
3.4 Low Fidelity Model	46
3.5 High Fidelity Model	48

4	Results	53
4.1	RVE	53
4.1.1	Low Fidelity Model 1: Thin Transverse Ply (2d=0.1mm)	54
4.1.2	Low Fidelity Model 2: transverse ply thickness 0.4mm	57
4.1.3	Low Fidelity Model 3: transverse ply thickness 1mm	60
4.1.4	Low Fidelity Model 4: thickest transverse ply (2d = 2 mm)	62
4.1.5	Results of Low Fidelity Model	64
4.2	Onset of Microcracking	65
4.2.1	High Fidelity Model 1	65
4.2.2	High Fidelity Model 2	67
4.2.3	Results of the onset of cracking	71
5	Conclusions	73
	Bibliography	75

List of Figures

1.1	Composite Material with unidirectional fibers [25]	10
1.2	Strength and Stiffness of composites materials and metals [25]	10
1.3	Stress strain curve for different kind of fibers [25]	12
1.4	Microstructure of graphite	13
1.5	The four phases during heat treatment [24]	13
1.6	Properties of Carbon-based Fibers [24]	14
1.7	Properties of Glass-based Fibers [24]	15
1.8	Use of Carbon-Fibres Reinforced Polymer in military and commercial aviation [28]	17
1.9	Materials used in the Boeing 787 Dreamliner (credit to <i>www.boeing.com</i>)	17
1.10	Average crack spacing as function of the applied stress with different transverse ply thicknesses [2]	19
1.11	Influence of the thickness on the onset of transverse cracking [6]	20
1.12	Crack propagation strain for notched and unnotched samples at different transverse ply thicknesses [11]	21
1.13	Microcraks density as function of the applied load [13]	22
2.1	Model of the fiber and matrix [27]	28
2.2	Normal stress and Shear stress distribution along the fiber[27]	30
2.3	Stress transmission in a cross-ply laminate [17]	31
2.4	Reference axis in a general composite structure	32
2.5	Failure tension in the 1 direction [24]	33
2.6	Failure in compression in the 1 direction [24]	34
2.7	Failure in tensile in the 2 or 3 direction [24]	35

2.8	Failure in compression in the 2 or 3 direction [24]	35
2.9	Failure in shear in the 2-3 plane [24]	36
2.10	Failure in shear in the 1-2 plane [24]	36
2.11	Example of failure in a composite laminate [26]	37
2.12	Schematic of the damage evolution in a cross-ply laminate [0/90/0] under a quasi-static load [18]	38
2.13	Possible delamination initiation mechanisms: a) initiation from the tips of a b) straight and c) branched transverse crack [18]	39
3.1	Systematic Transverse cracking phenomenon and isolation of RVE [?]	42
3.2	Modelling strategy flowchart	43
3.3	Crack Band Law in terms of stress and strain in the loading direction [23]	45
3.4	Low Fidelity Model	47
3.5	Boundary conditions of the model	47
3.6	High Fidelity Model	49
3.7	Boundary Conditions of the High Fidelity Model	50
3.8	Mesh of the High Fidelity Model	51
4.1	Cracking distance on [0 ₂ /90 ₄] specimen [15]	54
4.2	Low Fidelity Model 1	54
4.3	Cracks occurred in Model 1 with mesh size equal to 0.01mm	55
4.4	Cracks occurred in Model 1 with mesh size equal to 0.0075mm	56
4.5	Stress-Strain curves of two mesh size of Model 1	57
4.6	Low Fidelity Model 2	57
4.7	Cracks occurred in Model 2 with mesh size equal to 0.035mm	58
4.8	Cracks occurred in Model 2 with mesh size equal to 0.025mm	59
4.9	Stress-Strain curves of two mesh size of Model 2	59
4.10	Model 3	60
4.11	Cracks occurred in Model 3 with mesh size equal to 0.08mm	60
4.12	Cracks occurred in Model 3 with mesh size equal to 0.06mm	61
4.13	Stress-Strain curves of two mesh size of Model 3	61

4.14	Low Fidelity Model 4	62
4.15	Cracks occurred in Model 4 with mesh size equal to 0.2mm	62
4.16	Cracks occurred in Model 4 with mesh size equal to 0.1mm	63
4.17	Stress-Strain curves of two mesh size of Model 4	63
4.18	High Fidelity Model 1	65
4.19	Crack formation at the fiber-matrix interface	66
4.20	Crack formation and propagation through the thickness in Model 1	66
4.21	Stress-strain curve of the Model 1	67
4.22	High Fidelity Model 2	68
4.23	Crack formation at the fiber-matrix interface	69
4.24	Crack formation and propagation through the thickness in Model 2	70
4.25	Stress-strain curve of Model 2	70
4.26	71

Chapter 1

Introduction

1.1 Advanced Composite Materials

A composite is a material made by two or more different phases which can be distinguished with naked eye. These materials, if well designed, can exhibit the best qualities of their components.

We can find several types of composites materials, but this thesis focuses on fibrous composite. Fibers are very stiff and strong, but they are useless if there isn't something that holds them together. Long fibers are bounded together by another material called matrix.

The matrix, which has low density, stiffness and strength, is also needed to protect the fibers and to transfer stresses between broken fibers or fibers with a different orientation.

If the fibers are aligned, the combination between fibers and matrix create a material with a great stiffness and strength in one direction. Due to presence of low mechanical properties in the perpendicular direction with respect to the fibers orientation, usually laminates are made: layers, or plies, with different orientation are put together to make a unique structure which have good properties in all layers direction.

The invention of composite materials, which are advanced fiber reinforced materials, was a huge breakthrough in many sectors, as aerospace industry, automotive industry and wind energy, not only because of their high mechanical properties and low weight, but also for their superior resistance to fatigue cracking and corrosion by chemical agents.

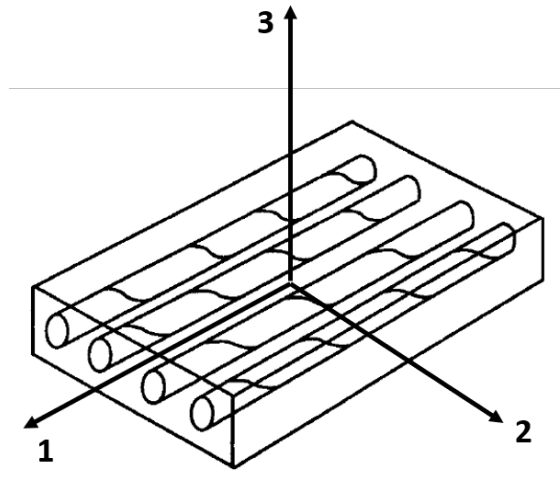


Figure 1.1. Composite Material with unidirectional fibers [25]

In the plot in 1.2 shows strength and stiffness of composite materials per unit weight.

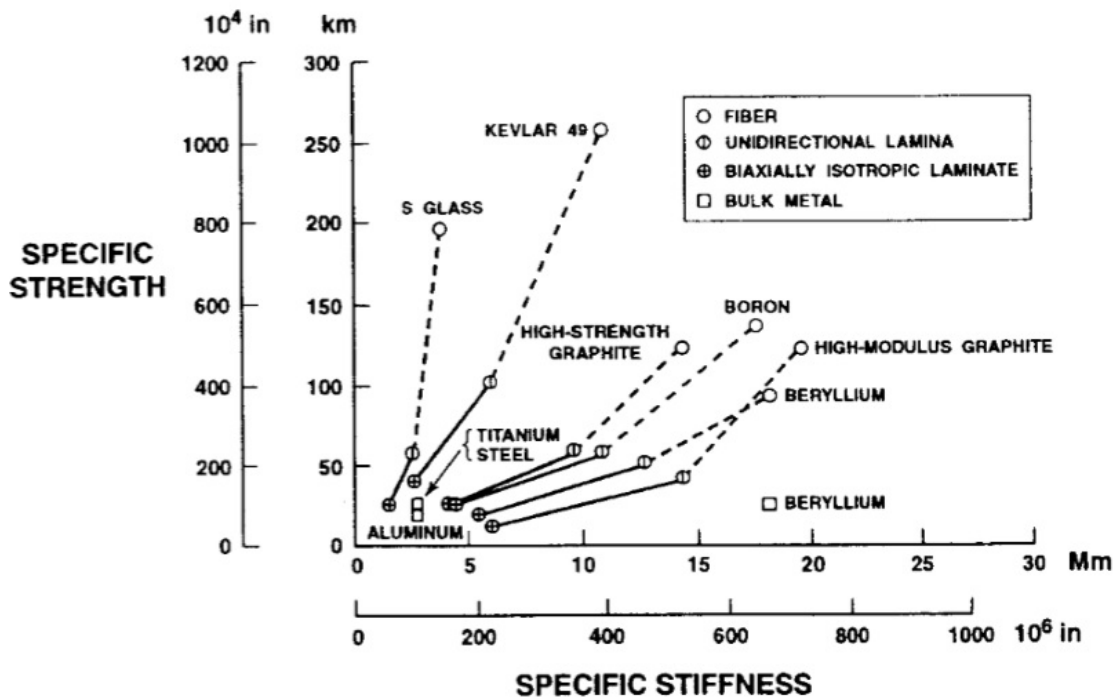


Figure 1.2. Strength and Stiffness of composites materials and metals [25]

1.1.1 Composite materials - Matrices

Fiber-reinforced material can be classified in different ways: the first subdivision is based on the type of the matrix, namely Metal Matrix Composites (MMC), Ceramic Matrix Composites (CMC), Polymeric Matrix Composites (PMC). This work focuses the attention on Polymeric Matrix Composites, whose the matrix is also known as resin; there are two kinds of resin: thermosets and thermoplastics.

Thermosets are chemically cross-linked and develop a network structure that, once they are cured sets the shape; thermosets cannot be remelted and begin to thermally decompose at high temperatures. Differently, thermoplastics can reversibly melt when heated and solidify when cooled. This means thermoplastics can be reshaped above a certain temperature and have the unique ability to be repaired one they have been placed into services. As a consequence, thermosets are more stiff, but less tough than thermoplastics, and have a brittle behavior.

Polymeric thermoset matrices are the most common in structural applications thanks to good mechanical properties, retention of mechanical properties when operating in hot and moist environments and good chemical resistance.

The most used resin is the Epoxy due to wide variety of properties: absence of volatile matters during curing, low shrinkage during curing, strong resistance to chemical and corrosion and the excellent adhesion. Moreover, epoxy has the capability to be partially cured and stored in this state, so that curing can be completed at later moment.

1.1.2 Composite materials - Fibers

Thermoset matrices can be reinforced by either polymeric or ceramics fibers: currently the common types are carbon, or graphite fibers, glass-based fibers and synthetic polymeric fibers, for example Kevlar. Picture 1.3 shows the stress-strain curve of different type of fibers ("B" means Boron fibers, "C" means Carbon fibers, "SiC" means Silicon Carbide).

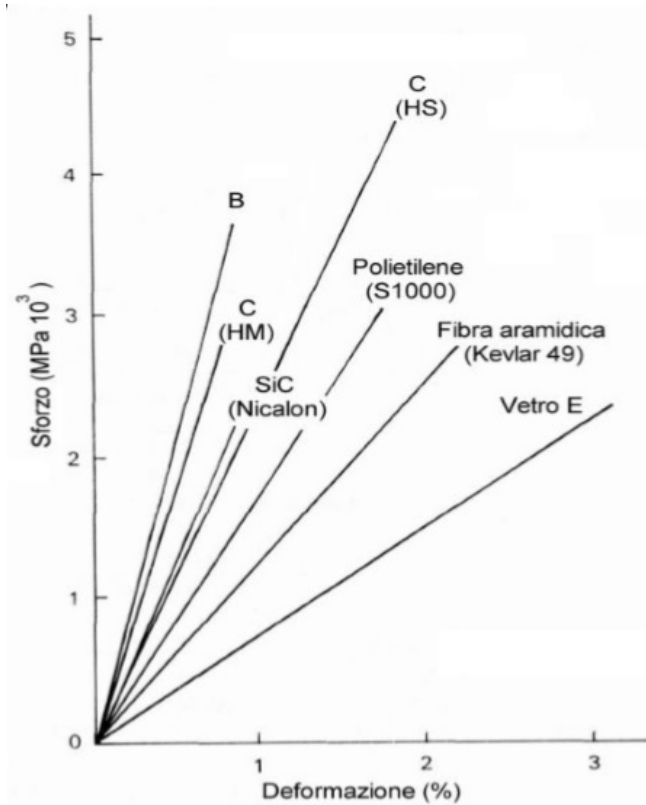


Figure 1.3. Stress strain curve for different kind of fibers [25]

Carbon Fibers

The precursor fibers are the starting point to make carbon-based fibers. The first precursor fibers were produced from rayon, but the fibers had a relatively low yield. Hence, nowadays, the precursors are made by either *PAN* (polyacrylonitril) or pitch. Ultimate fiber mechanical properties are not significantly affected by the type of precursors, but the manufacturing technique controls these properties, as it changes the microstructure of the fibers.

Graphite in its pristine form has a crystal form with planes of carbon atoms arranged in hexagonal unit cells, covalently bonded together. These planes are stacked upon each other to form a layered microstructure (fig 1.4): this conformation leads to a considerable lack of isotropy.

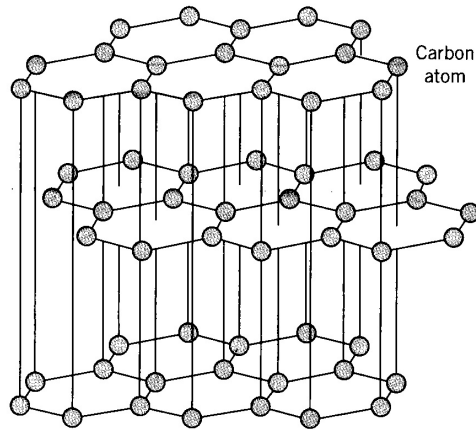


Figure 1.4. Microstructure of graphite

The ideal modulus in the axial direction (direction within the basal planes) is close to 1000 [GPa], but, due to various types of defects, the degree of orientation is lower. The problem can be fixed by stretching the fibers during graphitization and by increasing heat treatment temperature: this leads to increased stiffness in the axial direction. Figure 1.5 shows the four distinct phases during processing: it can be noted how the planes arrange themselves into an ordered and layered structure.

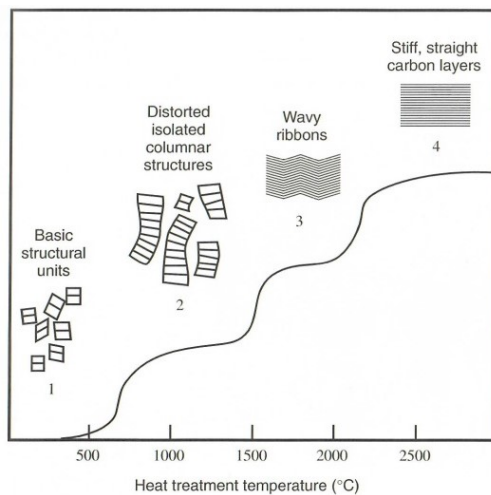


Figure 1.5. The four phases during heat treatment [24]

As mentioned before, manufacturing influences the fibers properties, especially in carbon fibers, where either high stiffness or high strength can be obtained. The different properties of carbon fibers are displayed in the table of figure 1.6, where can be noticed that, if high module is needed, there is a reduction of strength and vice versa. In the table, *IM* = intermediate modulus, *HM* = high modulus, *UHM* = ultra high modulus:

Properties of carbon-based fibers

Property	PAN			Pitch Type-P ⁴	Rayon
	IM ¹	HM ²	UHM ³		
Diameter (μm)	8–9	7–10	7–10	10–11	6.5
Density (kg/m^3)	1780–1820	1670–1900	1860	2020	1530–1660
Tensile modulus (GPa)	228–276	331–400	517	345	41–393
Tensile strength (MPa)	2410–2930	2070–2900	1720	1720	620–2200
Elongation (%)	1.0	0.5	0.3–0.4	0.4–0.9	1.5–2.5
Coeff. of thermal expansion ($\times 10^{-6}/^\circ\text{C}$)					
Fiber direction	–0.1 to –0.5	–0.5 to –1.2	–1.0	–0.9 to –1.6	—
Perpendicular to fiber direction	7–12	7–12	—	7.8	—
Thermal conductivity ($\text{W}/\text{m}/^\circ\text{C}$)	20	70–105	140	—	38
Specific heat ($\text{J}/\text{kg}/^\circ\text{K}$)	950	925	—	—	—

Figure 1.6. Properties of Carbon-based Fibers [24]

Glass-Based Fibers

Glass fibers are generally lower performers compared to graphite fibers, but considerably cheaper and easier to study because of their isotropic behavior. Despite the advent of higher performance fibers, Glass-fiber Reinforced system are responsible of the majority of polymer matrix composite market.

Silica (SiO_2) constitutes the basis of all most common glass-based fibers. After heat treatments, silica can be used as glass in many applications. Due to the high temperature needed to produce glass and

to shape it, other type of glasses were developed to decreased the complexity of the processing:

- Type A: first to be used, it's currently employed in few minor applications.
- Type E: was developed for better resistance to attack by water and mild chemical concentrations.
- Type C: has a much improved durability when exposed to acids and alkalins.
- Type S: developed for high performance applications, is the type with the highest stiffness and strength

Figure 1.7 details the physical and mechanical properties of the most common glass fibers:

Properties of glass-based fibers

Property	Glass type		
	E	C	S
Diameter (μm)	8–14	—	10
Density (kg/m^3)	2540	2490	2490
Tensile modulus (GPa)	72.4	68.9	85.5
Tensile strength (MPa)	3450	3160	4590
Elongation (%)	1.8–3.2	4.8	5.7
Coeff. of thermal expansion ($\times 10^{-6}/^{\circ}\text{C}$)	5.0	7.2	5.6
Thermal conductivity ($\text{W}/\text{m}/^{\circ}\text{C}$)	1.3	—	—
Specific heat ($\text{J}/\text{kg}/^{\circ}\text{K}$)	840	780	940

Figure 1.7. Properties of Glass-based Fibers [24]

1.2 Applications of advanced composite materials

The market of advanced composite materials involves many sectors, as aerospace industry, automotive industry, wind energy, naval industry and many others. According to the American Composites Manufactures Association, in 2017 the market of glass fibers reached 2.5 billion pounds in terms of composites materials produced. The demand of carbon fiber was approximately 75000 metric tons.

1.2.1 Aerospace applications

The biggest breakthrough was in the aerospace aviation, where using composites materials aircraft can save lots of weight: the large tail of the B777 was made by carbon-fiber/epoxy, it was estimated that the weight saving was from 15% to 20%.

Experience with B777 proves that composite structures required less scheduled maintenance than non composite structures: the tail of this aircraft was 25% bigger than the aluminum tail of B767, yet it required 35% fewer scheduled maintenance labor hours. This reduction is due to the reduced risk of corrosion and fatigue of composites compared to metals.

The used of composites happened gradually, the first stage was the replacement pieces, then companies started the production of pieces where a plane was design from the beginning to have various parts in fiber reinforced composite materials. Nowadays, aircraft are made with more then 50% of composites, as for example the B787 Dreamliner (1.9).

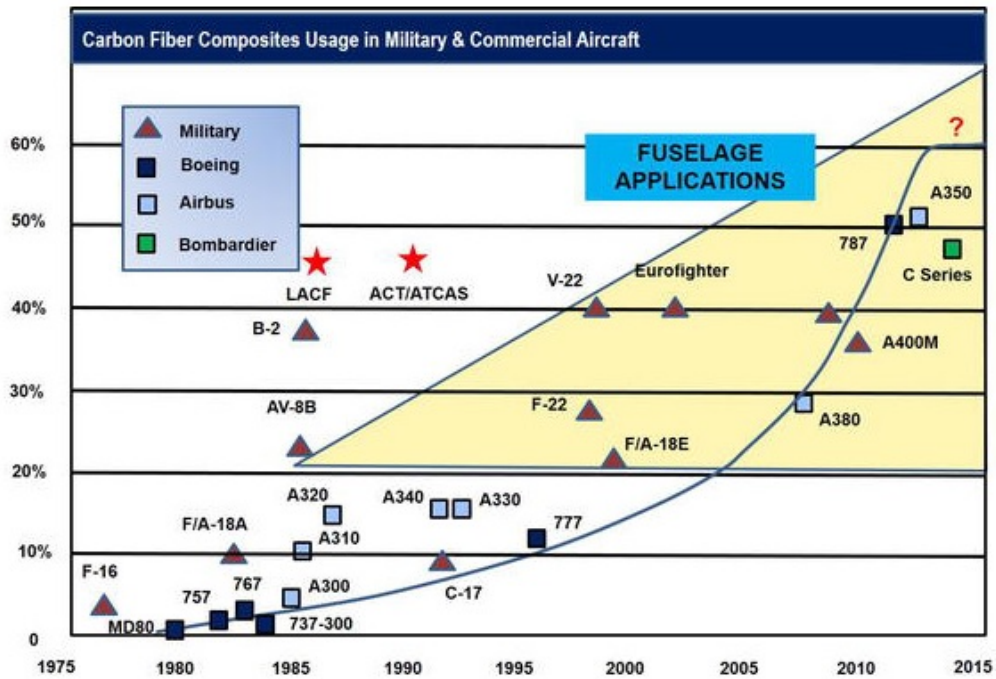


Figure 1.8. Use of Carbon-Fibres Reinforced Polymer in military and commercial aviation [28]

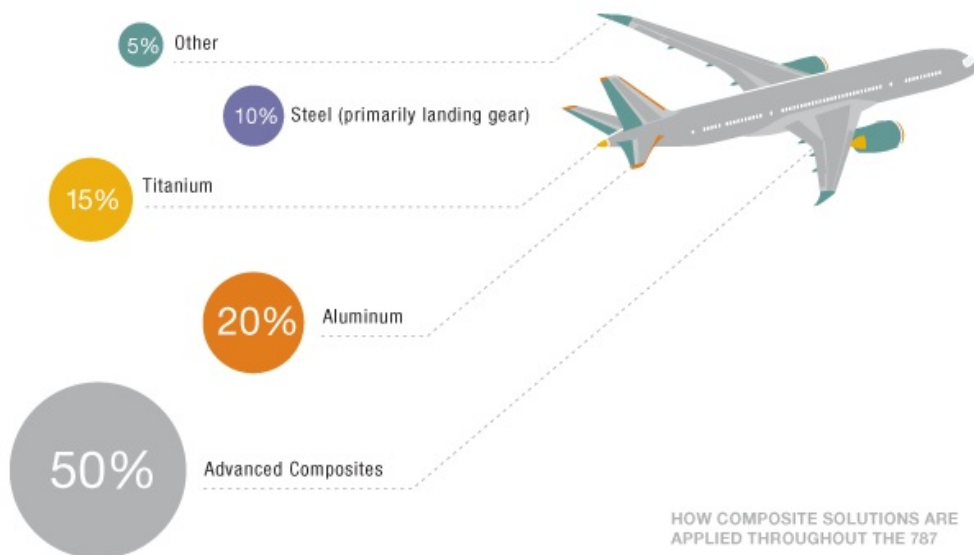


Figure 1.9. Materials used in the Boeing 787 Dreamliner (credit to www.boeing.com)

1.2.2 Wind energy applications

Wind energy is a market in expansion all over the world, as lots of countries aim to reach the independency from fossil fuel. In order to satisfy the high request of wind energy generation, reliable and long living turbine has to be produced.

Wind turbine are usually subjected complex, multiaxial, cyclic loading and they are often exposed to moisture, water and bad condition for long period. Due to the high cost of repair and maintenance, the biggest part of wind blades is made by glass-fibers or carbon-fibers/epoxy.

Glass fibers are cheaper than carbon fibers and therefore are used for producing blades, which length is up to 100 meters.

1.3 Motivation

As discussed in the previous section, composite materials are widely used, even if the failure mechanism is not completely understood. For this reason, in order to avoid catastrophic events, high Safety Factors (SF) are applied. As a consequence, composite structures are built using more material than necessary, obtaining heavier components; in the aerospace field, more weight means more fuel requested, which implies higher costs. Damage initiation and propagation, which are essential for design, production and health monitoring of structures, are important topics and they are still object of studying.

The first form of damage in a laminate is usually matrix microcracking, or transverse cracking, which is the formation of cracks in the transverse ply in a direction parallel to the fiber of that ply and perpendicular to the load applied. Cracks initiate first, then combine and propagate until they reach to the ply boundaries, at which point local micro-delamination is triggered. Delamination become dominant after the saturation of crack density until the catastrophic failure.

The study of microcracking started in the 70's with the observation on initiation and propagation of the transverse cracks. *Laws and Dvorak* [1] presented a model for transverse cracking based on statistical fracture mechanics, through which they analyzed the loss of stiffness and progressive cracking, providing a formulation for the displacement

field between cracks.

Garrett and Bailey [2] saw that cracks show a systematic crack spacing, which depends on the applied stress and transverse ply thickness. From experiments on composites made by polyester resin and unidirectional glass cloth, it was understood that crack spacing becomes bigger by increasing either applied stress or transverse ply thickness (fig. 1.10)

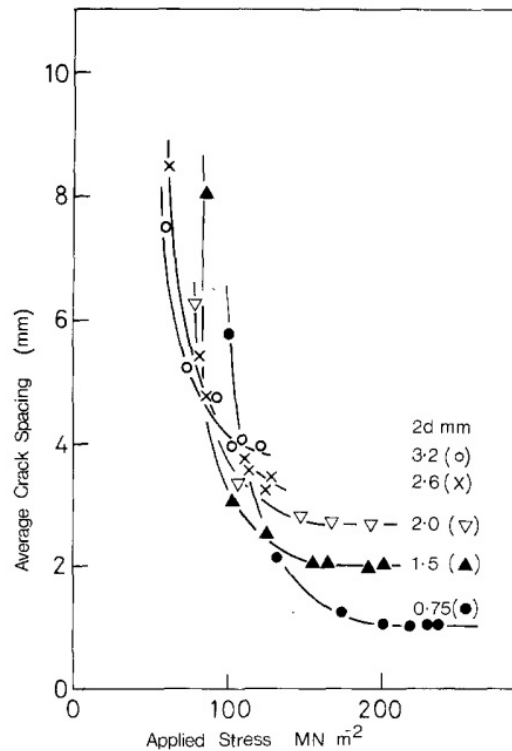


Figure 1.10. Average crack spacing as function of the applied stress with different transverse ply thicknesses [2]

Other papers (*Parvizi and Bailey* [3], *Stevens and Lupton* [4]) agree with *Garrett and Bailey* and try to find additional theories to predict the crack spacing: as example, *Peters and Chou* [5] applied the Weibull theory to the probability of failure considering the distortion of the stress field due to cracks.

Experiments about the influence of transverse ply thickness on the strength were first carried out by *Parvizi et Al.*[6]: they tested a series of $[0/90_n]_s$ laminates of glass fiber-reinforced epoxy with the thickness

of the outer plies constant (equal to 0.5 [mm]) and the thickness of the inner ply ranging from 0.1 [mm] to 4 [mm]. The results obtained (fig 1.11) show that their prediction works for thin plies, while, for thicker plies, the failure strain is underestimated. As a matter of fact, the trend is that, after a certain thickness (in this case 0.4 [mm]), the strain of failure becomes approximately constant at the value of unconstrained transverse ply.

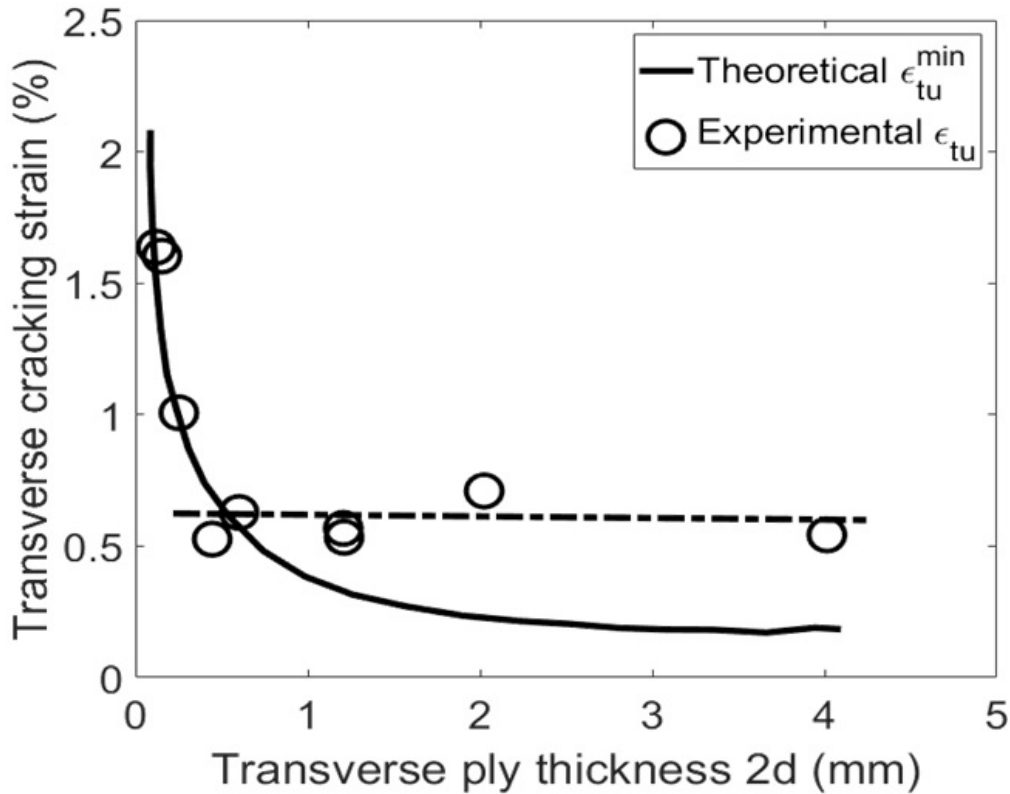


Figure 1.11. Influence of the thickness on the onset of transverse cracking [6]

The cracking phenomenon, explained with the shear lag theory, is also different depending on the thickness of the samples: in specimens with transverse thickness greater than 0.4 [mm], the majority of the cracks, after reaching the critical value, propagate instantaneously and span whole inner ply; in specimens with transverse thickness ranging from 0.15 to 0.4 [mm], cracks appear at the edges of the inner ply, then grow very slowly to vary length; differently in specimens with transverse

thickness smaller than 0.15 [mm], transverse cracking were not observed prior to the complete failure of the specimen.

This study was confirmed by later works: especially *Garcia et Al.* [7] were able to reproduced the trend, noticing that in the thin ply specimens both delamination and transverse cracking occur and the same time.

Flaggs and Kural [8] found out that experiments on $[0/90]_s$ laminates prove the analytical model provided by *Parvizi et Al.*[6], which is less accurate with $[\pm\theta/90]_s$ laminate.

Many studies with the purpose of explaining the difference between the analytical model and the experiments were made and some of which, like *Nairn* [9] and *Flaggs* [10], could reduce the gap between predictions and experimental results using variations in the shear lag model, but nonone was able to find a solution.

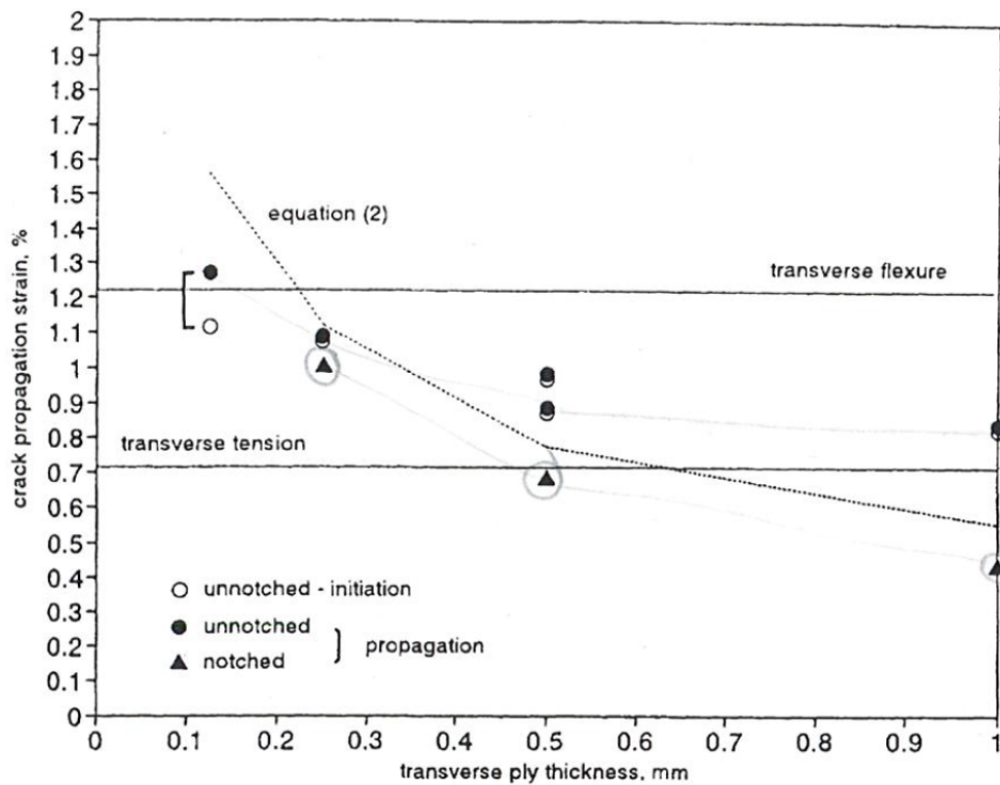


Figure 1.12. Crack propagation strain for notched and unnotched samples at different transverse ply thicknesses [11]

Later on, *Boniface et Al.*[11] thought that the issue was the assumption of implicit presence of initial defects spanning the entire ply. Based on the fact that the flaws, greater than a few ply thickness, would propagate with lower strain, while smaller cracks length would require higher strain for propagation (*McCartney, 1995* [12]), *Boniface et Al.* separated crack initiation and propagation stages using notched and unnotched samples made by Carbon Fiber-Reinforced epoxy. Results are reported in the figure 1.12.

In the specimen with greater thickness, crack initiation and propagation in the unnotched samples happen at the same time, while the crack propagation in notched samples is smaller: this implies that crack initiation has a fundamental role in its propagation.

Differently, thin samples show that the initiation of the crack occurs at smaller strain, this means that the propagation of the crack controls the phenomenon.

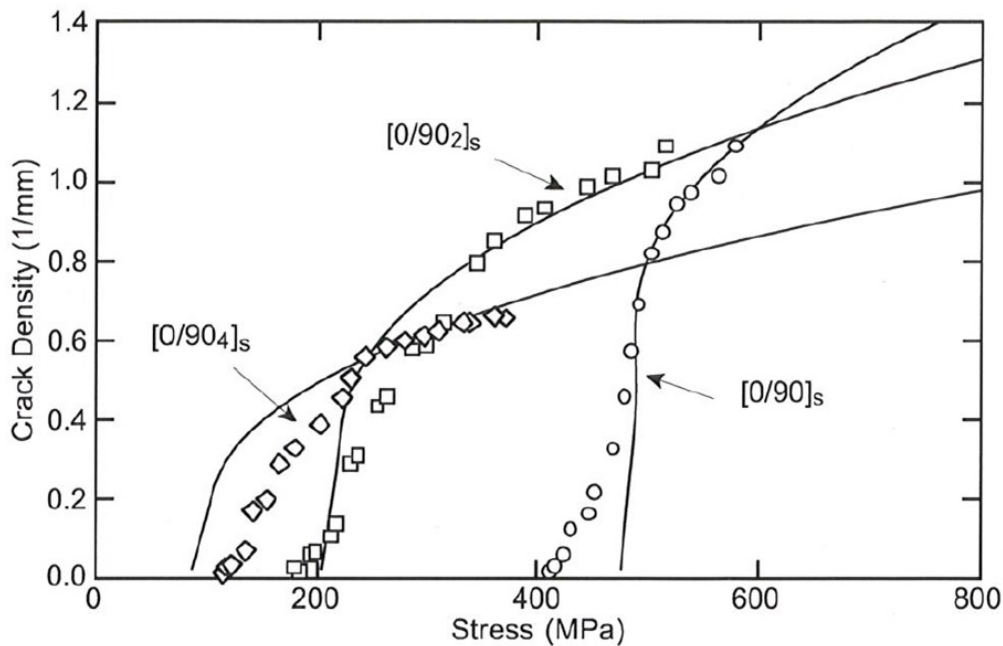


Figure 1.13. Microcracks density as function of the applied load [13]

As explained above, cracks initiate in the transverse layers and have

an intensive propagation until the where delamination becomes dominant: this point is called saturation point of crack density; crack density, according to *Nairn* [13], increases rapidly, then it slows until the saturation point. The trend is similar in for the different $[0/90_n]_s$ layups, regardless of the thickness of the transverse ply.

The onset of transverse cracking occurs first in thicker plies than in thinner one: in fact, thinner plies develop more microcracks and have an higher saturation point. It was also proved by *Sun et Al.* [15], *Herraez et Al.* [14], *Sabey et Al.* [16] that the trend is the same for both Carbon-fibre Reinforced and Glass-fibre Reinforced .

After the first crack, the stiffness of the laminate doesn't change much, because the zero plies are absorbing most of the load, but the more the progressive transverse cracking increases, the more the stiffness of the laminates decreases. Different trends were seen based on experiments: *Sun et Al.* [15] found out that the reduction was independent from the transverse ply thickness, but *Herraez et Al.* [14] discovered that thicker laminates have the same stiffness reduction, while for thinner laminates the reduction of the modulus with the applied strain is more limited. Probably, *Sun et Al.* couldn't catch this difference because they considered three different $[0/90_n]_s$ layups, with $n = 2,3,4$, with only big thickness.

Sabey et Al. [16] carried out more precise experiments, considering four different sequences of plies: $[\pm 45/90]_s$, $[\pm 45/90_2]_s$, $[\pm 45/90_4]_s$, $[0_2/90_4]_s$. Results show that the slope of the normalized stiffness curve changes at the initiation of full width transverse cracks and the reduction continues until cracks density saturation point. The reduction is different for all layups, but the trend is similar.

A different trend is showed by $[\pm 45/90]_s$: onset accumulation of observed cracks do not alter the decay rate of the stiffness and transverse cracks are only in the free edges and don't propagate through the entire width.

Transverse tensile strength is taken as the stress for the onset of full width transverse cracks. *Dvorak and Laws* [17] were able to find two analytical equations, one for thick and one for thin transverse plies, to predict the strength. The model used by them, differently from *Parvizi et Al.* [6], assumes the existence of a critical crack length (δ_c), which

governs the crack growth. Below the critical size of length, transverse cracking grow in a stable manner, but once the cracks reach the critical value, their growth becomes governed by the classical Griffith Criterion.

Dvorak and Laws showed that in thick plies the initial flaw, where the crack initiate, is not affected by the presence of adjacent plies, because, being a material property, it is much smaller than the thickness of the ply. Being aware that a crack in a thick ply first spans the thick than the width, the strength can be written:

$$\sigma_{cr} = \sqrt{\frac{2G_{IC}}{\pi\Lambda^0\delta_C}}$$

where G_{IC} is the critical energy release rate, δ_c is the critical size of the cracks, $\Lambda^0 = 2\left(\frac{1}{E_T} - \frac{\nu_L^2}{E_L}\right)$, E_L the stiffness in the direction of transverse ply fibers, ν_L the Poisson ratio and E_T the stiffness in the direction of the thickness of the transverse ply.

For thin transverse ply, the initial flaw is as big as the thickness ($2d$), so that crack can propagate just through the width and the strength is related to the onset of microcracking in the width direction. The strength can be written as:

$$\sigma_{cr} = \sqrt{\frac{4G_{IC}}{\pi\Lambda^0 a\xi_I}}$$

where ξ_I is a coefficient which takes into account the influence of the constraining plies on the stress field.

The aim of this work is to create a virtual model which characterizes the failure behavior for an *in situ* ply, taking into account the influence of the thickness of the transverse ply. A detailed model is built on the FEM software ABAQUS, in order to study in detail the onset of transverse cracking, which starts from the defects presents in the material or from the matrix-fibers interface.

The failure behavior is studied on a cross ply laminate loaded with a tensile stress in the zero plies direction. The ninety ply is modeled at the microscale with random fibers depicted, and a damage model, based on the Crack Band method proposed by Bazant and Oh [20],

which preserves mesh objectivity, is applied to both the *in situ* ply and the Zero plies.

Chapter 2

Failure of composites Laminates

This chapter analyzes the failure problem in laminates, focusing on Polymer Matrix Composites (PMC). To understand the failure mechanism, the first step is to become confident with the stress field in a laminate, predicted by the Shear Lag Theory.

2.1 Shear Lag Theory

The Shear Lag model was first proposed by *H.L. Cox* [22] in 1952 and was focused on the transfer of the tensile stress to fiber via interfacial shear stress. Considering one circular fiber surrounded by the matrix (fig. 2.1a), where the vertical lines are for reference), when an external load is applied, fig. 2.1b in the fiber direction, a shear distortion of the matrix close to the fiber can be seen.

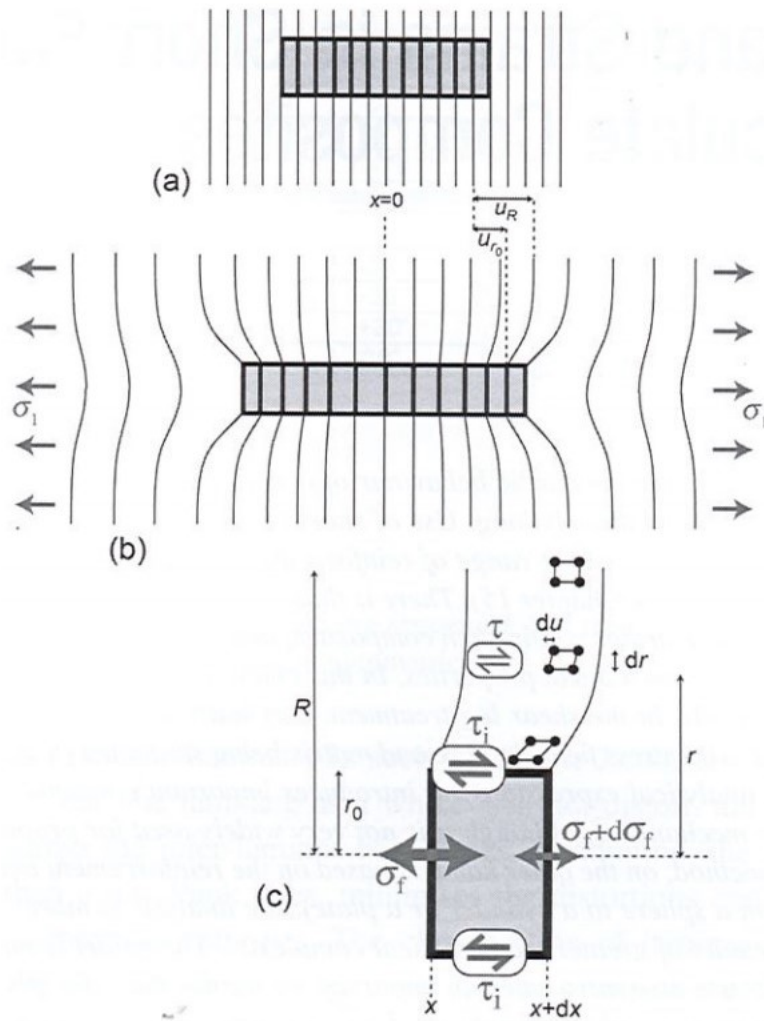


Figure 2.1. Model of the fiber and matrix [27]

Focusing on one element of the distorted configuration (fig. 2.1c), the equilibrium equation can be written:

$$-(\pi r_0^2)d\sigma_f = \tau_i(2\pi r_0 dx) \quad \text{hence} \quad \frac{d\sigma_f}{dx} = \frac{-2\tau_i}{r_0}$$

the interfacial shear stress τ_i is obtained by considering how the shear stress in this direction varies within the matrix as function of radial position:

$$\tau = \tau_i \frac{r_0}{r}$$

the shear strain can be written both as variation of the displacement in the loading direction "u" with the radial position and in terms of local shear stress and shear modulus of the matrix "G_m":

$$\gamma = \frac{\tau_i(r_0/r)}{G_m} \quad \gamma = \frac{du}{dr}$$

Equalizing and integrating the equation, an expression for the shear stress may be found:

$$\tau_i = \frac{(u_R - u_{r_0})G_m}{r_0 \ln(R/r_0)}$$

where R is the far field radius where the matrix strain has become effectively uniform ($du/dr \approx 0$) and it's affected by proximity of neighboring fibers and hence the fibers volume factor. Giving that $(\frac{R}{r_0}) \approx \frac{1}{f}$, than:

$$\frac{d\sigma_f}{dx} = \frac{-2(u_R - u_{r_0})G_m}{r_0^2 \ln(1/f)}$$

Rewriting displacements $\frac{du_{r_0}}{dx} = \epsilon_f = \frac{\sigma_f}{E_f}$ and $\frac{du_r}{dx} = \epsilon_1$, the resulting equation is as follow:

$$\frac{d^2\sigma_f}{dx^2} = \frac{n^2}{r_0^2}(\sigma_f - E_f\epsilon_1)$$

where \mathbf{n} is a dimensionless constant $n = \sqrt{\frac{2E_m}{E_f(1+v_m)\ln(1/f)}}$.

This is a second order linear differential equation of standard form, which has a solution $\sigma_f E_1 \epsilon_1 + B \sinh(nx/r_0) + D \cosh(nx/r_0)$, and, applying the boundary conditions $\sigma_f = 0$ at $x = \pm L$ (L is the fiber half length), the final expression for the variation of both normal and shear stress may be found:

$$\sigma_f = E_f \epsilon_1 \left[1 - \cosh\left(\frac{nx}{r_0}\right) \operatorname{sech}(ns) \right]$$

$$\tau_i = \frac{E_f n \epsilon_1}{2} \sinh\left(\frac{nx}{r_0}\right) \operatorname{sech}(ns)$$

The variations of the stress along the fiber depends on the his length, as can be seen from the plots in fig. 2.2. The important thing to understand is that when a laminate is loaded in the direction of fibers, these absorb most of stress and they transmit it to the matrix by shear stress.

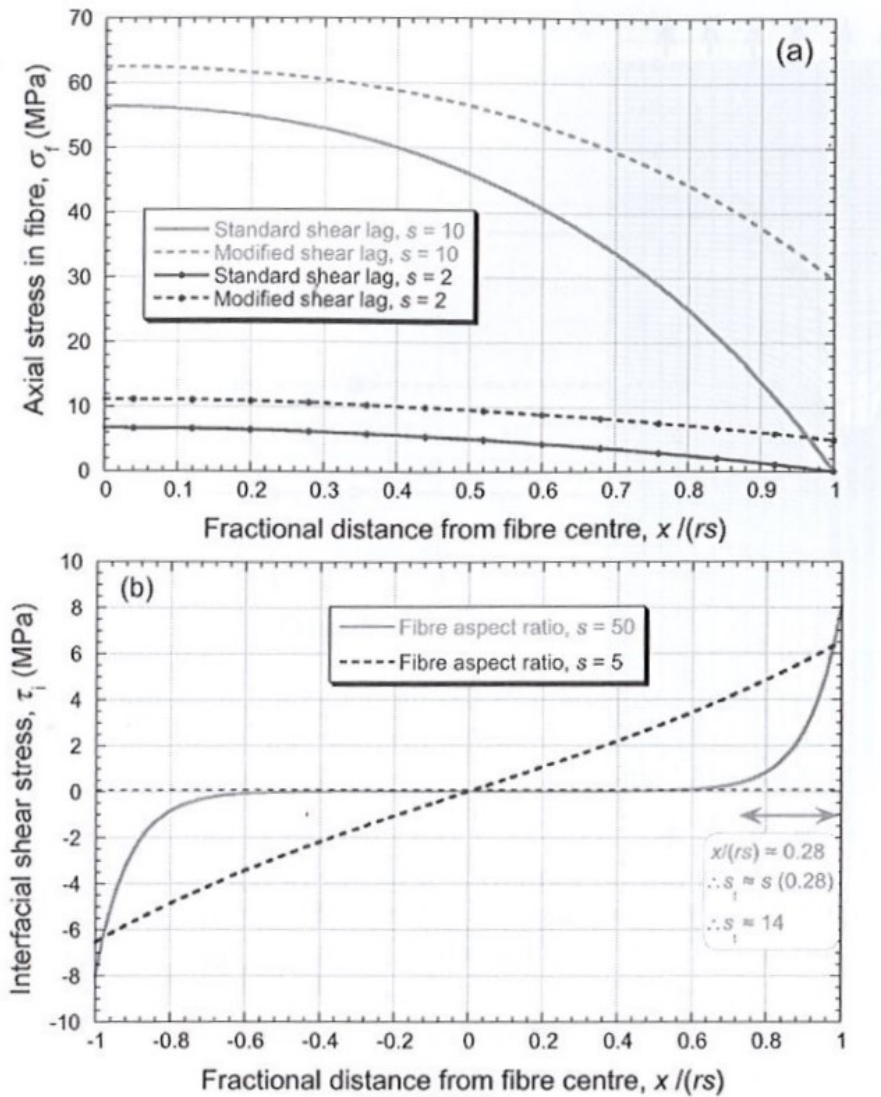


Figure 2.2. Normal stress and Shear stress distribution along the fiber[27]

Considering a laminate with two outer plies with fibers in the direction of the load and one ply with fibers in perpendicular direction, the outer plies fibers absorb most of the load applied to the structure and

transmit it to transverse ply by the shear stress. Figure 2.3 shows the stress transmission between layers, considering that the stress applied $\sigma_a = \frac{b\sigma_l + d\sigma_t}{b+d}$, b is the height of the longitudinal plies, d is the half height of the transverse ply:

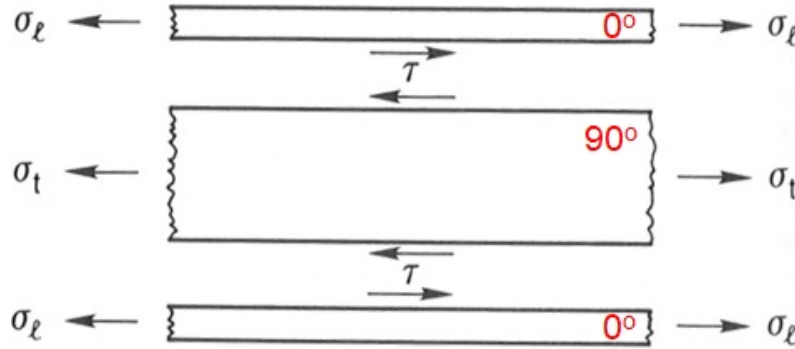


Figure 2.3. Stress transmission in a cross-ply laminate [17]

2.2 Failure in composites

As reported in the Hyer's book [24], "failure is considered to be the loss of integrity of the material itself". The failure is not necessarily a catastrophic event, but it implies a load redistribution within the structure or permanent deformation; the structure can be still functional to limited degree.

Failure for fiber reinforced materials in both tensile and compressive loading is a complex topic and it's function to the direction of the applied load with respect to the direction of the fibers. For this reason, tensile failure in the fiber direction is controlled by fiber strength, while tensile failure perpendicular to the fibers is controlled by the strength of the matrix and the bond between fibers and matrix. Hence, six kind of failure are taken into consideration:

- Fiber failure due to tensile load
- Fiber failure due to compressive load
- Composite failure due to tensile load in transverse direction

- Composite failure due to compressive load in transverse direction
- Composite failure due to shear stress in the 1-2 plan
- Composite failure due to shear stress in the 1-2 plane

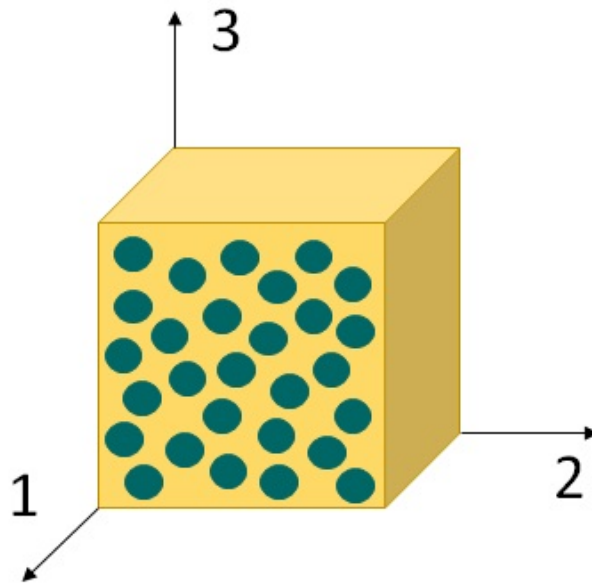


Figure 2.4. Reference axis in a general composite structure

Fiber failure due to tensile load

If the loading is in the direction of the fibers, the important parameter is the strength of the fibers (denoted as σ_1^T). When a fiber is overloaded, it breaks and the load is transferred by the matrix to the neighboring fibers through shear stresses. As the load increases, more fibers fail and more load is absorbed by integer fibers: the surrounding matrix material cannot sustain the load, so the failure propagates rapidly with the increasing load.

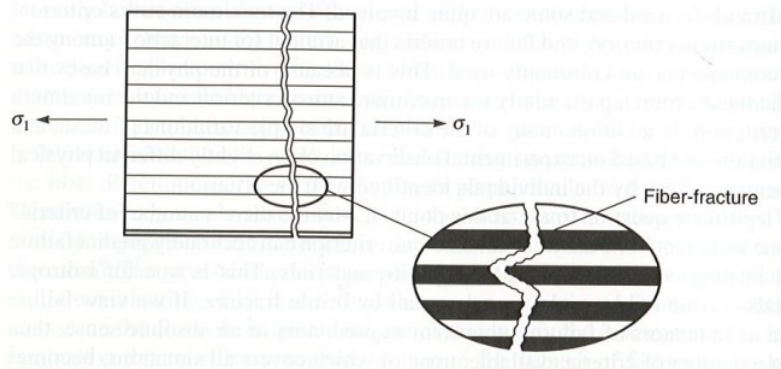


Figure 2.5. Failure tension in the 1 direction [24]

Fiber failure due to compressive load

With a compressive stress in the fibers direction, composites fail by fiber kinking or microbuckling. Kinking occurs among localized groups of fibers and the fibers in the band fracture at both ends of the kink. The fracture inclination angle " β " can vary from 10 to 30 degrees and the kink band " W " is usually equal to 10 to 15 fiber diameters.

The mechanism responsible for this behavior is the yielding or softening of the matrix as the stresses on it increase to suppress fiber buckling. The fiber-direction compressive strength σ_1^c is influenced by the fibers misalignment and the yielding of the matrix follows the relation:

$$\sigma_1^c = \frac{G_{12}}{1 + \phi/\gamma_{12}^Y}$$

where ϕ is the angle of the initial misalignment and γ_{12}^Y is the shear strain at which the shear stress-strain relation loses validity due to softening effects in the matrix.

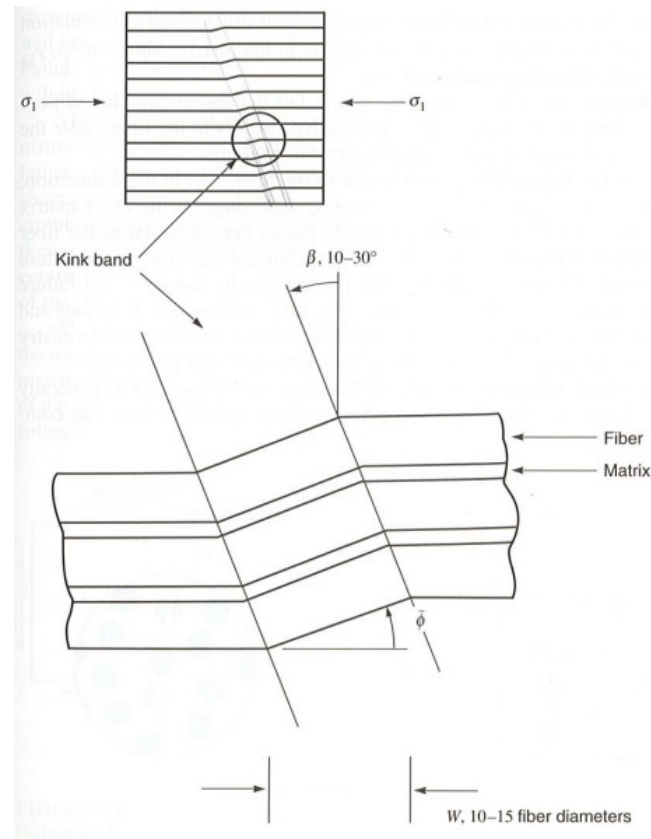


Figure 2.6. Failure in compression in the 1 direction [24]

Composites failure due to tensile load in transverse direction

A load applied in a direction perpendicular to fiber can produce failure in three ways: tensile failure of the matrix material, tensile failure of the fiber across its diameter and failure of the interface between fibers and matrix. The second type of failure is the probable, especially for glass fibers which are isotropic, while the last type of failure is the more catastrophic, because it indicates that fiber and matrix are not well bounded.

The first type of failure is the most interesting for this research and it depends on the matrix strength σ_2^T or σ_3^T .

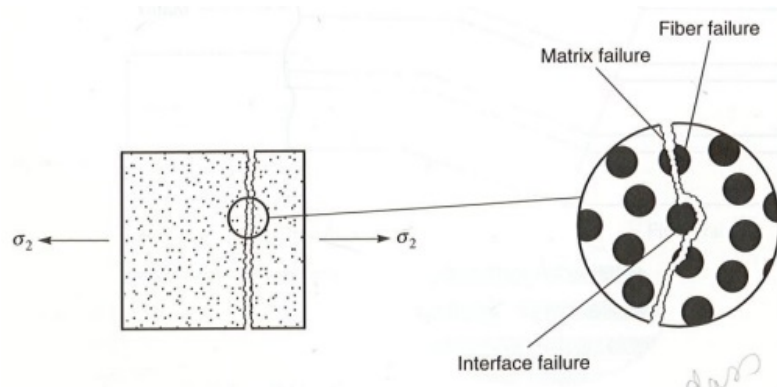


Figure 2.7. Failure in tensile in the 2 or 3 direction [24]

Composites failure due to compressive load in transverse direction

The failure in compression perpendicular to fibers is due to material crushing and interacting. The compressive strength σ_2^C , or σ_3^C , it's usually greater than tensile strength σ_2^T .

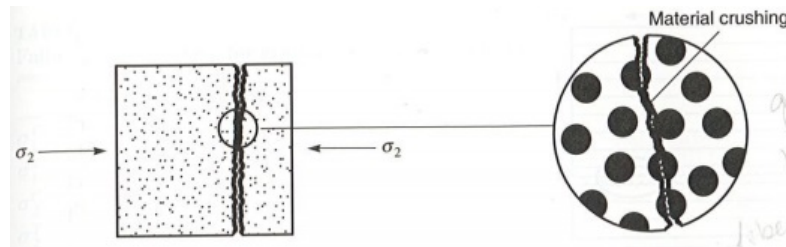


Figure 2.8. Failure in compression in the 2 or 3 direction [24]

Composites failure due to shear stress in the 2-3 plane

The shear strength τ_{23} in the 2-3 plane is limited by the same mechanism that governs tensile strengths perpendicular to fibers. The shear stress produces a tensile stress on a plane oriented at 45° . The micromechanisms limit the performance of the material. Moreover, the shear strength is independent from the sign of the shear stress.

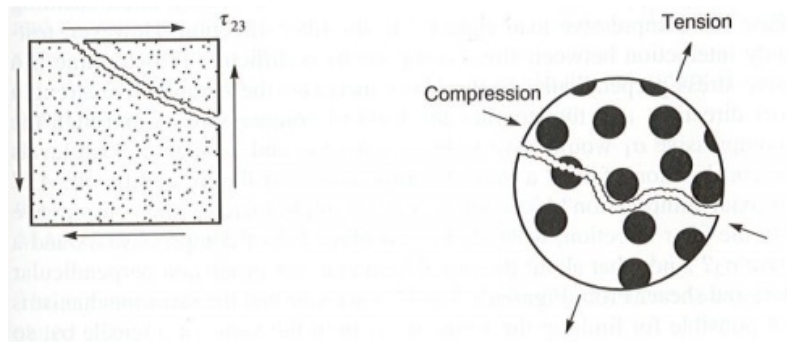


Figure 2.9. Failure in shear in the 2-3 plane [24]

Composites failure due to shear stress in the 1-2 plane

The failure in the plane 1-2 is caused by the shear separation of the fiber from the matrix along the length of the interface. The shear strength in this plane is equal to the strength in the plane 1-3

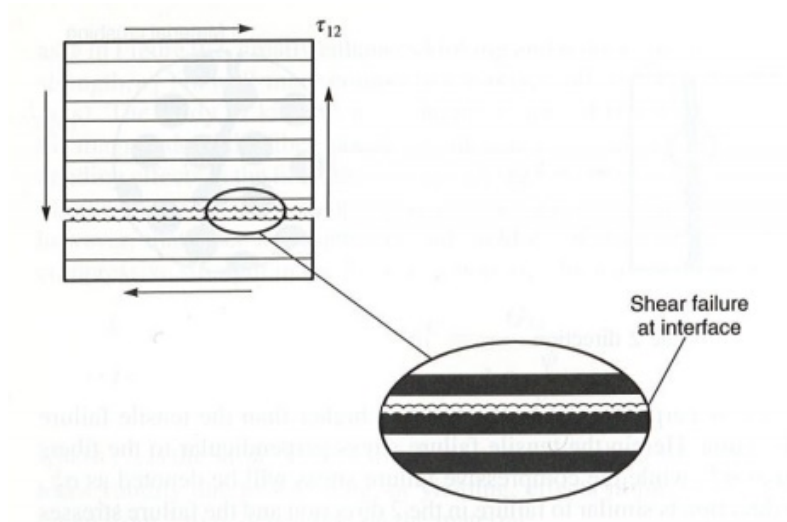


Figure 2.10. Failure in shear in the 1-2 plane [24]

2.3 Delamination

In the previous section, we have discussed the failure of an individual lamina. In case of a multi-ply structure, the failure of one lamina (first ply failure) doesn't necessarily lead to the failure of the entire laminate, but it degrades the mechanical properties. The ultimate load-carrying capacity of the laminate can be much higher than the first ply failure load.

Considering a laminate with several plies in several direction, the failure of the structure is the result of the failure of many layers, from the weakest to the strongest, as shown in picture 2.11, At every ply failure, stiffness is reduced and the stiffness matrix must be modified.

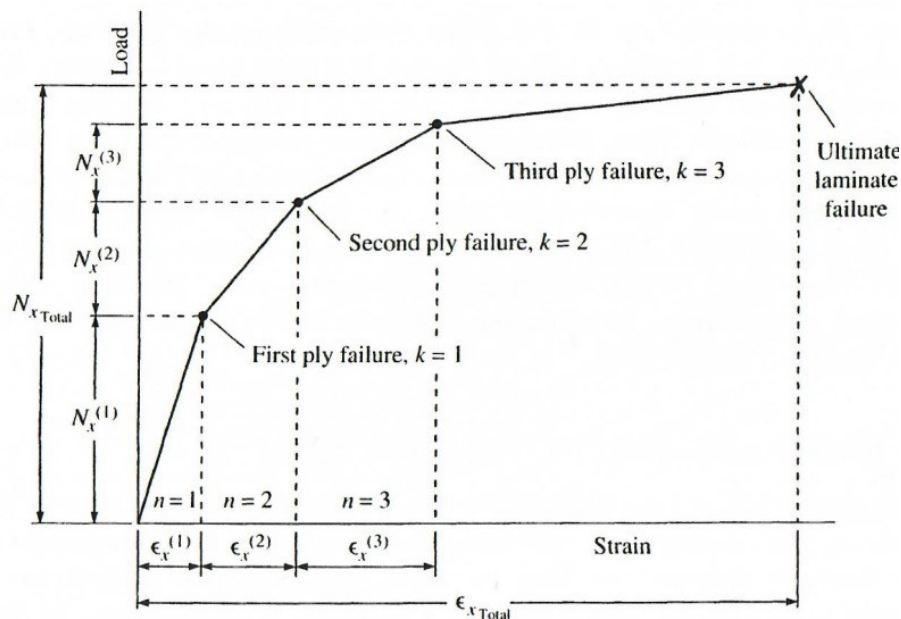


Figure 2.11. Example of failure in a composite laminate [26]

Differently from the other phenomena, delamination, the origin and growth of crack on the interface of different orientation plies, it is one of the dominant failure mechanisms in composite laminate and it can contribute to the complete failure of structural components. The initiation and growth of delamination, which can arise under both static

and fatigue loading, is often preceded and triggered by matrix transverse cracking.

Considering a $[0_m/90_n]_s$ under tensile load in the zero plies direction, the first event of damage is the formation of transverse matrix cracks in the 90° plies, growing across the whole ligament. Increasing the applied load results in a multiplication of transverse cracks and in the onset of micro-delaminations at the layers interface, reasonably promoted by the singular stress field arising close to the tip of transverse cracks.

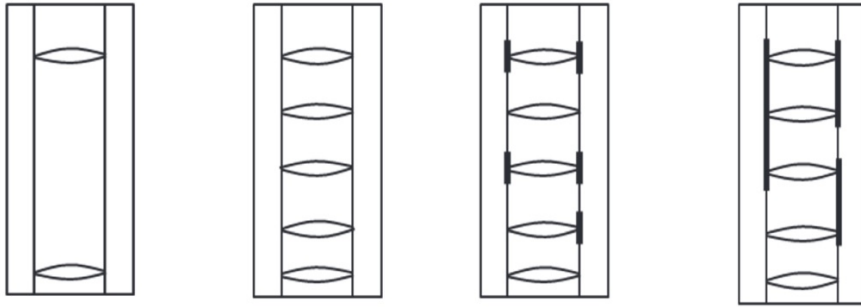


Figure 2.12. Schematic of the damage evolution in a cross-ply laminate $[0/90/0]$ under a quasi-static load [18]

The onset set of delamination is driven by stresses in the close neighborhood of transverse cracks tip along the interface. Their intensity can be quantified using the Generalized Stress Intensity factor K_1 , K_2 and K_3 . Considering the simple case of a laminate under a tensile load N_y transverse to the crack faces, K_1 is the only parameter to quantify the local stress field and the onset of delamination happens when $K_1 = K_{1c}$, meaning the critical value.

According to the work of *Carraro et Al.* [18], who studied the problem for two different lay-ups ($[0/90_2]_s$ and $[0_2/90_4]_s$), the three different scenarios reported in fig. 2.13 can trigger the onset of delamination from transverse cracking:

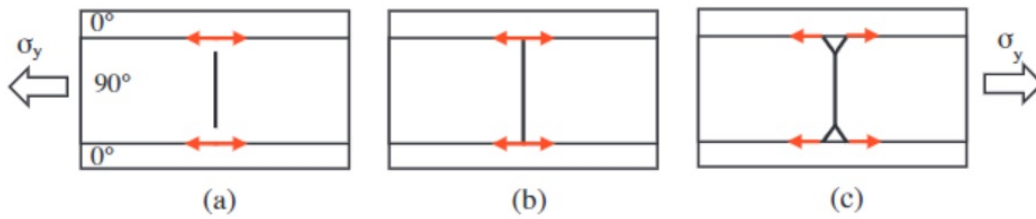


Figure 2.13. Possible delamination initiation mechanisms: a) initiation from the tips of a b) straight and c) branched transverse crack [18]

In the first scenario called *Cook-Gordon mechanism* (fig. 2.13a), the delamination initiates before the transverse crack tip reaches the interface. A crack propagates towards a bi-material interface, the peak value of the radial stress along the crack bisector is located at a certain distance from the crack tip. As a crack approaches an interface, the peak value can be at the interface itself and the delamination can start before the crack reaches it.

However, in the authors' opinion, the inter-laminar and the intra-laminar strength and toughness of composite laminates are, reasonably, similar, as both are controlled by the matrix and the fibre-matrix interface. Therefore, the initiation of a delamination is not expected to occur according to the Cook-Gordon mechanism. Moreover, this mechanism was never observed in the specimens tested during the present experimental campaign.

The most common mechanism of crack initiation are 2.13b and 2.13c: the transverse cracks reach the interface in a either straight or branched configuration and delaminations initiate. Some experiments showed delaminations without the presence of transverse cracks; usually this is due to the presence of irregularities on the edge surfaces.

Carraro et Al. [18] also investigated the evolution of the total transverse crack density under tensile load: the initiation of delamination is reported (vertical lines) and the onset is much higher in the laminate with tinnier transverse ply.

The crack formed due to delamination are not critical until they start linking the tips of the transverse cracks: after a critical value is reached, the propagation is very rapid and the failure occurs in a short time.

Chapter 3

Finite Element Method Model

This chapter is dedicated to the creation of the FEM model, made with the Finite Element software ABAQUS.

3.1 Representative Volume Element

The computational cost is a very important factor in finite element simulations: models with a high number of degrees of freedom require the creation of a representative volume element (RVE), as modeling the entire structure is too expensive in term of calculation and time. The RVE is the smallest portion of the laminate with the same characteristics and properties: to recreate the entire structure is enough to put together several RVE.

In order to find the length of RVE, a property of composite materials has been used: according to the shear lag theory, when a cross-ply laminate $[0/90_n]_s$ is loaded in the direction normal to fiber in the transverse ply, the zero plies absorb most the load and transmit to the matrix by the shear stress. When stress in the matrix reaches a critical value, a crack occurs: while the load is increasing, more cracks occur and the distance between them is a characteristic distance called shear lag distance. Shear Lag distance between cracks is constant as it has fix geometry and fix properties.

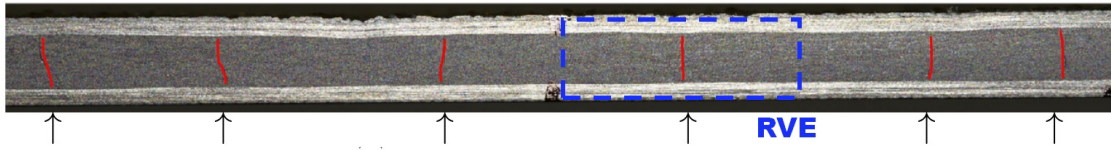


Figure 3.1. Systematic Transverse cracking phenomenon and isolation of RVE [?]

Picture 3.1 show cracked transverse ply of a specimen. The smallest portion of the structure that can repeated to recreate the laminate, namely the specimen, is this one with crack in the middle and with a length of " $2h$ ", which is the distance between cracks and it will be the length of the RVE.

3.2 Modelling strategy

The value of " h " depends by many factors and cannot be found in literature. This thesis uses another approach, displayed in the flowchart in picture 3.2.

The first step is to create a big model of the laminate at the macroscale, which means that, instead using fibers and matrix, plies are made with orthotropic homogenized materials. This model is called "Low Fidelity Model" because it doesn't give information on crack propagation through the thickness, but shows the spots where cracks occur.

The second step is to run an analysis with the failure model and find the cracking distance, also called shear lag distance. The failure model must be mesh independent.

The third step is to create the *High Fidelity Model*, that is the RVE with the Ninety ply with fibers and matrix depicted. The length of this model will be equal to the shear lag distance, while the other dimensions remain the same of the Low Fidelity Model. The last step includes the study of the High Fidelity Model, which provides information about crack formation and propagation in the ninety ply.

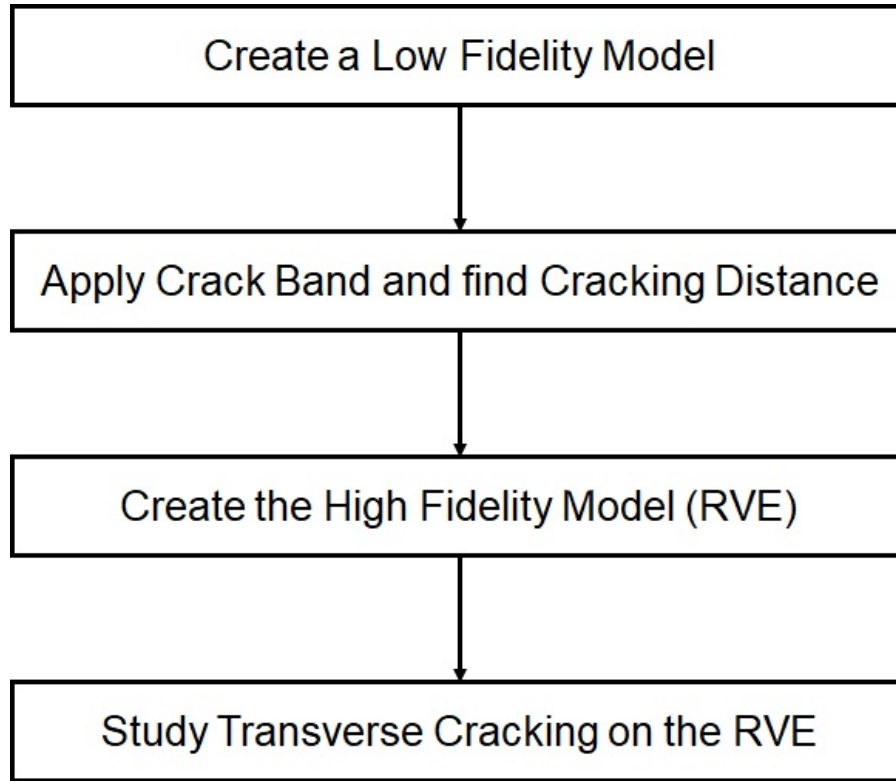


Figure 3.2. Modelling strategy flowchart

3.3 Damage model

3.3.1 Hashin's Failure Criteria

The Hashin's Criteria [19] suites perfectly composite materials because it separates fiber and matrix failure modes and distinguishes tensile states from compressive states. Hashin proposed one different expression for each case, considering the different stresses that take part to the degradation of the composite material.

Here, the cases to evaluate are the Longitudinal Fibers Mode and the Tensile Matrix Mode. The first one will be applied to the zero plies, where the failure mode is the fibers failure:

$$\frac{(\sigma_{11})^2}{T_{11}^2} + \frac{(\sigma_{12}^2 + \sigma_{13}^2)}{S_{12}^2} = 1$$

where T_{11} is the longitudinal tensile strength and S_{12} is the longitudinal shear strength in the "12" direction, which is equal to the strength in the "13" direction for orthotropic materials.

Tensile Matrix Model will be applied to the ninety plies and the expression, considering the reference axis in picture 2.4, is:

$$\frac{(\sigma_{22} + \sigma_{33})^2}{T_{22}^2} + \frac{\sigma_{23}^2 - \sigma_{22}\sigma_{33}}{S_{23}^2} + \frac{(\sigma_{12}^2 + \sigma_{13}^2)}{S_{12}^2} = 1$$

where T_{22} is the transverse tensile strength and S_{23} is the transverse shear strength in "23" direction.

3.3.2 CrackBand Model

The Crack Band model based on the one proposed by **Bazant and Oh** [20] is used to model the damage and failure of the RVE. The model assumes that when the critical load is reached, microcracks appear and the additional opening due to cracking is smeared over a band of material, in our case over an element.

Using Hashin's failure Criteria, a single critical load is not provided, but the failure occurs when the equation presented in the previous section is satisfied. Picture 3.3 shows the model of the failure of one element.

Once the Hashin's equation is satisfied, σ_{cr} is set as the highest stress in the loading direction reached and ϵ_{cr} is the corresponding strain. After this point, the traction-separation law controls the damaging of the element, namely of the material.

The softening regime is followed by multiplying the Young's Modulus by a stiffness reduction factor D until the maximum separation $\delta_f = h\epsilon_f$ is reached. Here h is the characteristic length of the element which preserves mesh objectivity [21] and ϵ_f is the complete failure strain of the material.

The energy dissipated under mode I cracking, which is a properties of the material is given by:

$$G_{Ic} = \int_0^{\delta_f} \sigma(\delta)d\delta = h \int_0^{\epsilon_f} \sigma(\epsilon)d\epsilon$$

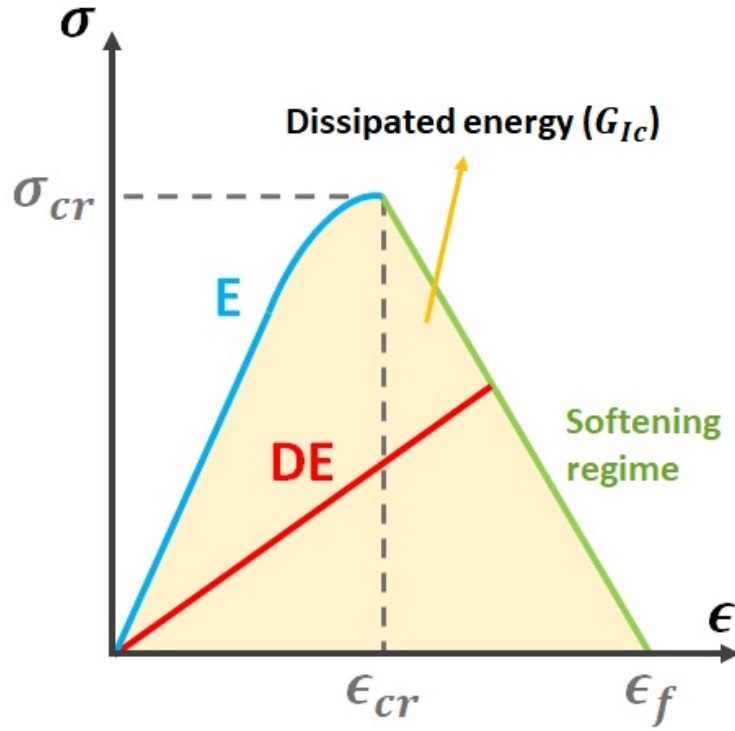


Figure 3.3. Crack Band Law in terms of stress and strain in the loading direction [23]

In order to preserve mesh objectivity, the G_{Ic} has to be normalized for each element so that $g_{Ic} = \frac{G_{Ic}}{h}$ is the area under the $\sigma - \epsilon$ curve. Hence, the complete failure strain, after which in the model there's the deletion of the element, is computed by:

$$\epsilon_f = 2 \frac{G_{Ic}}{\sigma_{cr} h}$$

The stiffness reduction factor D is given by:

$$D = \frac{\sigma_{cr}}{(\epsilon_f - \epsilon_{cr})E} \left(\frac{\epsilon_f}{\epsilon} - 1 \right)$$

where ϵ is the actual strain in the loading direction. D ranges from 1 to 0, where $D = 1$ means there is no damage, $D = 0$ corresponds to complete failure.

3.4 Low Fidelity Model

The Low Fidelity Model is modeled with homogeneous orthotropic materials, reported in the following table. The material used are Fiber Glass-E and Epoxy Resin RIM 135 / RIMH 1366 and the volume fraction of the fibers is equal to 55%:

Longitudinal Tensile Modulus (E_1)	41000	[MPa]
Transverse Tensile Modulus ($E_2 = E_2$)	11000	[MPa]
Poisson Ratio (ν_{12})	0.26	
Transverse Tensile Strength (T_{11})	1060	[MPa]
Transverse Tensile Strength (T_{22})	36	[MPa]
Transverse Shear Strength (S_{23})	38	[MPa]
Longitudinal Shear Strength (S_{12})	45	[MPa]
Critical Energy Release Rate (G_{Ic})	0.06	[J/mm ²]
Density (ρ)	$1.9e^{-9}$	[Kg/mm ³]

The model of the cross ply laminate is showed in the figure [3.4](#):

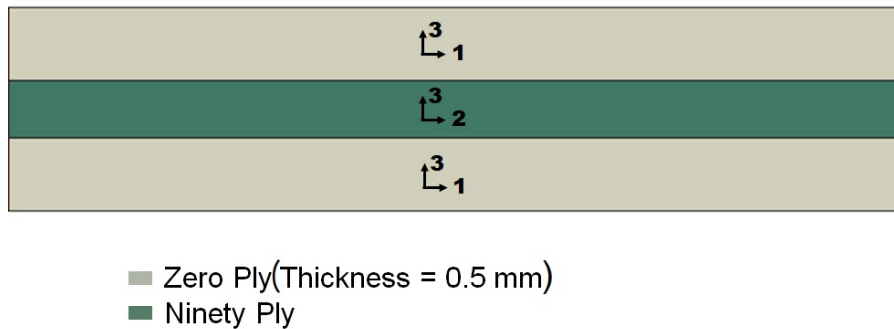


Figure 3.4. Low Fidelity Model

Figure 3.5 shows the boundary conditions of the model. The displacements of the bottom face in y direction is set to zero, as the displacement of the behind face in z direction. Due to the tensile velocity applied on both sides of the model, there is no need to constrain the displacements in x direction, so the rigid motion of the model is prevented:

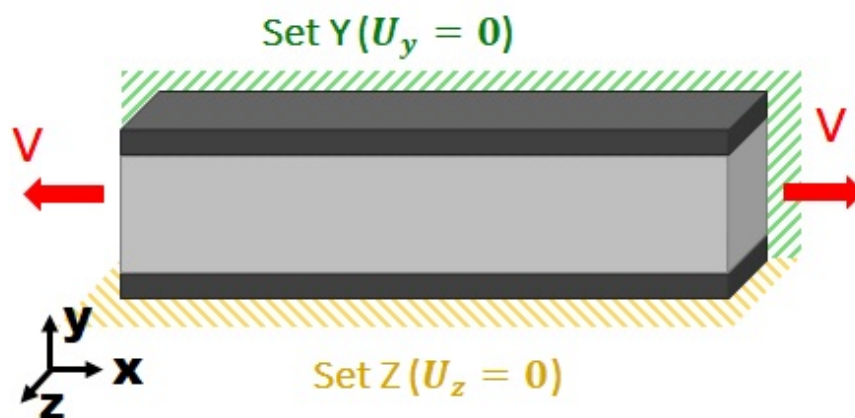


Figure 3.5. Boundary conditions of the model

Two subroutines were used for zero plies and ninety ply, due to different kind of failure. The difference between these two subroutines, which both use the Crack Band Model, is the failure equation. Even if the failure of the longitudinal plies is not in the scope of this work, a failure mode is applied to be sure not to reach the breaking of the laminate

and to have a reliable delamination phenomenon. The Criteria applied is the Hashin Criteria, shown in section 3.3.1, but longitudinal plies to fail need to satisfy the Longitudinal Fibers Mode equation, while the transverse ply requires the Tensile Matrix Mode equation.

3.5 High Fidelity Model

The High Fidelity Model (picture 3.6) takes into account the matrix and fibers in the ninety ply. The Zero Plies are modeled as the Low Fidelity model and they have the same properties. In the next table, properties of matrix and fiber are reported:

Fiber Glass-E		
Young's Modulus ($E_1 = E_2 = E_2$)	73000	$[MPa]$
Poisson Ratio (ν_{12})	0.28	
Density (ρ)	$2.55e^{-9}$	$[Kg/mm^3]$
Radius (r)	0.007	$[mm]$

Epoxy Resin RIM 135 / RIMH 1366		
Young's Modulus ($E_1=E_2 = E_2$)	2495	[MPa]
Poisson Ratio (ν_{12})	0.37	
Density (ρ)	$1.7e^{-9}$	[Kg/mm ³]
Tensile Strength (σ_{cr})	64	[MPa]

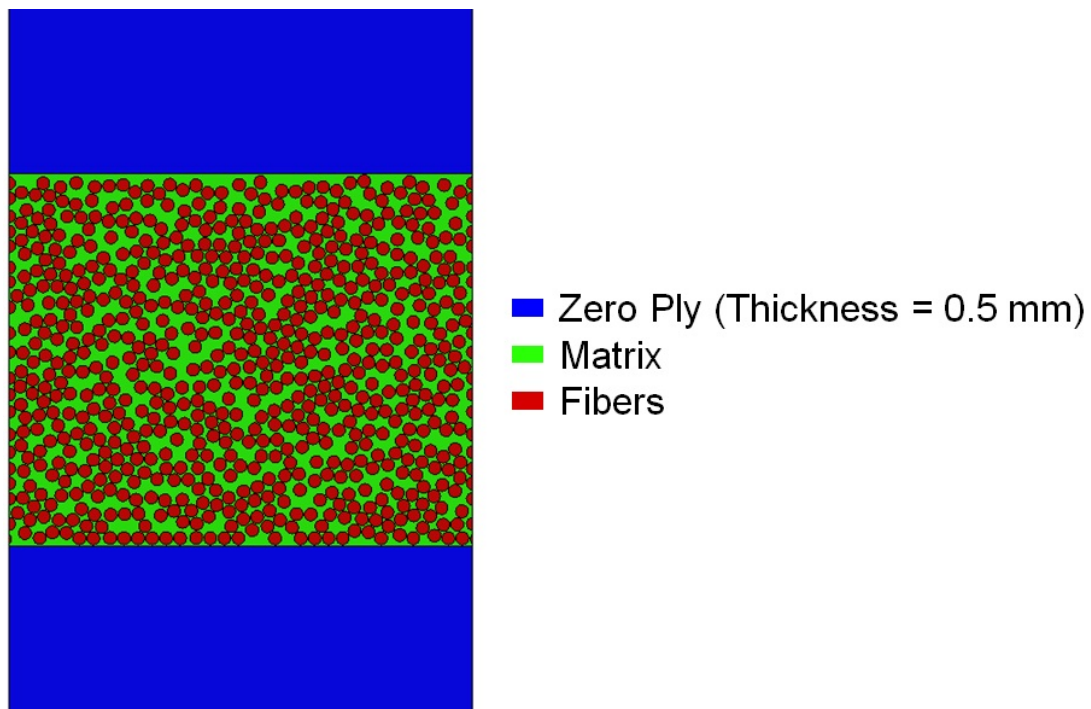


Figure 3.6. High Fidelity Model

The model, showed in figure 3.7, is constrained in z and y direction as

the Low Fidelity Model. Along x direction a velocity is applied directly to the model, because the periodical boundary conditions ensure the lack of boundary effects.

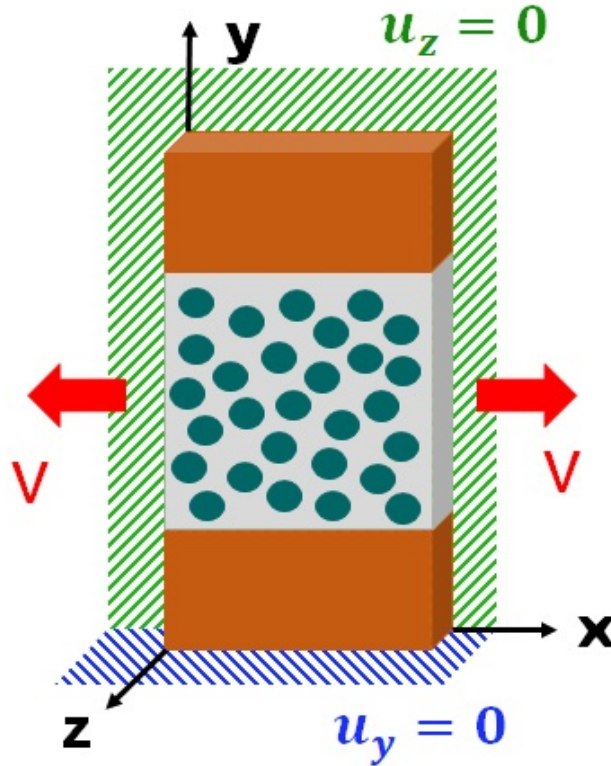


Figure 3.7. Boundary Conditions of the High Fidelity Model

Fibers are placed Randomly in the ply and the minimum distance between them is equal to the radius divided by 7. The position of the fibers is provided by a MATLAB script, which take as input the dimension of the ninety ply and the volume fraction. In order to create periodical boundary conditions, the fibers on the edges are symmetrical.

After placing the correct number of fibers, the geometry on ABAQUS is created by a Python script. The mesh of the ninety ply is as big as the minimum distance between fibers in order to have at least one element between them. The zero plies are meshed with bigger size, as their role is just to constrained the transverse ply and there is no need of high precision. Detail of the mesh can be seen in the following figures:

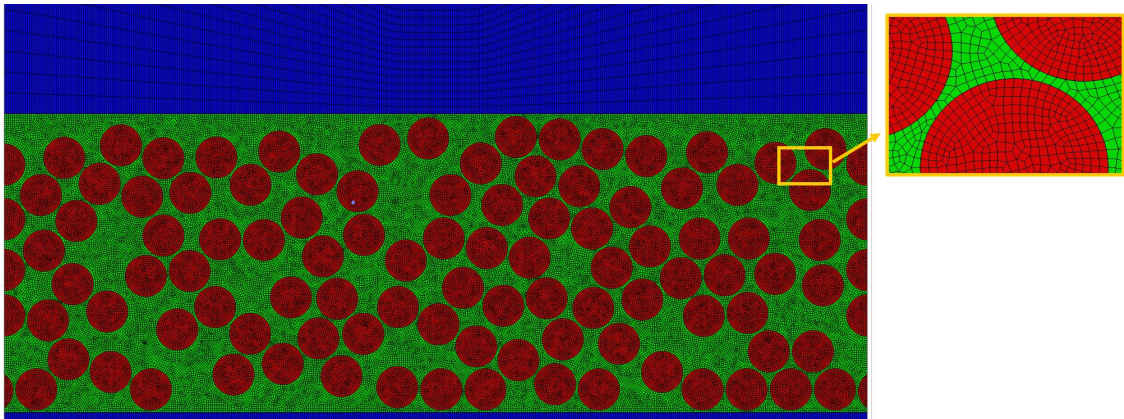


Figure 3.8. Mesh of the High Fidelity Model

In the High fidelity model, the failure Criteria is just applied to the matrix and the longitudinal plies. For the matrix, which is an isotropic material, the Maximum Stress Criteria is enough to explain the failure mode. For the zero plies, as in the Low Fidelity Model, the Hashin Criteria with the Tensile Fibers Mode equation is used.

Chapter 4

Results

This chapter describes the results of the FE analysis. Four models were created. While the thickness of the longitudinal plies was set constant to $b = 0.5 \text{ mm}$, the thickness of the transverse ply was chosen different for each model:

Model	Ninety Ply Thickness
MODEL 1	0.1 [mm]
MODEL 2	0.4 [mm]
MODEL 3	1 [mm]
MODEL 4	2 [mm]

4.1 RVE

The homogenized model presented in the previous chapter is used to find the length of the RVE. In order to prove the mesh objectivity of the failure subroutine, every laminate is analyzed on with two different mesh size. The two model don't always fit perfectly due to numerical reasons, but the cracking sequence and the cracks spot is always similar.

Experiments performed by *Sun et Al.* on Carbon Fiber Epoxy laminate provide an idea of the length of the cracking distance. The specimen shown in figure 4.1 is a $[0_2/90_4]$ with ply thickness of 0.18mm . The average cracking distance is 1.6 mm , which is similar to the transverse ply thickness ($2d = 1.44\text{mm}$).

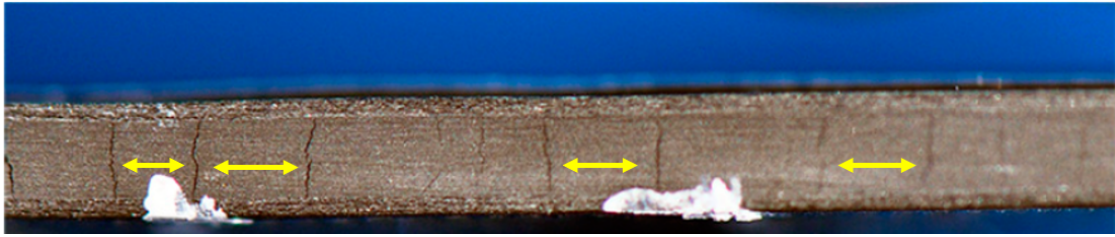


Figure 4.1. Cracking distance on $[0_2/90_4]$ specimen [15]

4.1.1 Low Fidelity Model 1: Thin Transverse Ply ($2d=0.1\text{mm}$)

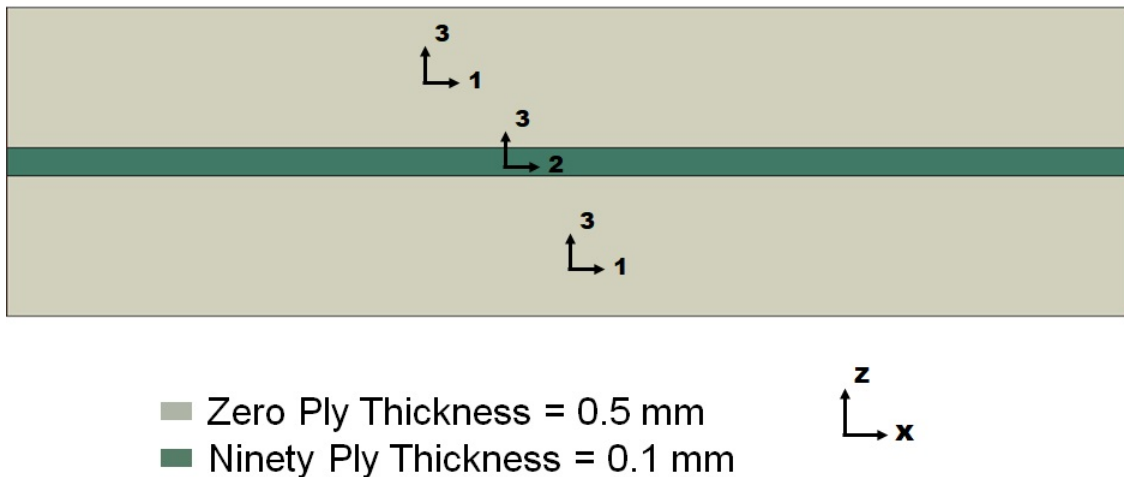


Figure 4.2. Low Fidelity Model 1

The Model 1, shown in picture 4.2, has the thinnest transverse ply thickness. Tests were performed with two mesh sizes of the 8-node brick elements (C3D8): the first one with a size of 0.01 mm, the second with a size of 0.0075 mm.

Due to numerical reasons, in the results of the model, cracks can be visualized as line spanning the entire ply or as a bunch of defects occurring at the same time. For this reason, the crack spot is marked with a red dashed line.

Considering the first test in Model 1, from a homogeneous field of

stress, two cracks symmetrical with respect to the center of the model occur at the same time (fig. 4.3a). Then other defects occur at the average distance of 0.2 mm (4.3 b and c). All the cracks are symmetrical with respect to the center of the model, due to symmetrical boundary conditions of the model. The stress plotted in the picture, σ_{11} , is the one in the loading direction, which corresponds to the x direction.

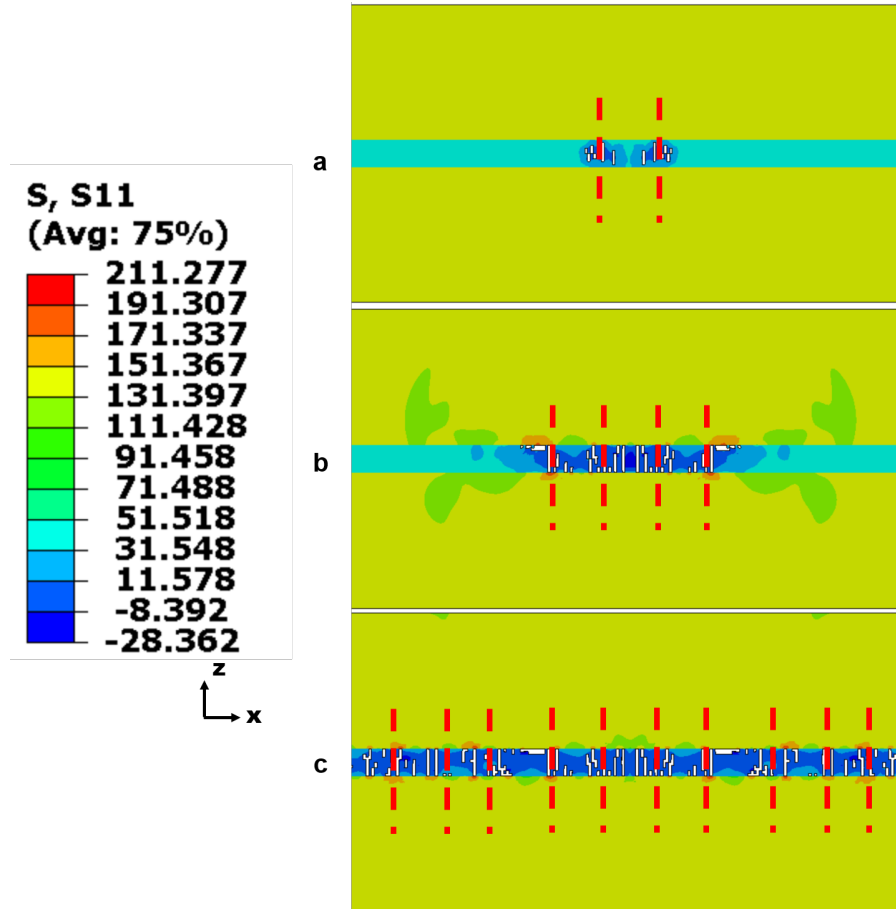


Figure 4.3. Cracks occurred in Model 1 with mesh size equal to 0.01mm

In the second test of Model 1 (mesh size of 0.0075 mm), the cracking sequence, reported in picture 4.4, is the same of the previous one with more defects. Moreover, the average distance between cracks correspond to the Shear Lag Distance of the first test of Model 1.

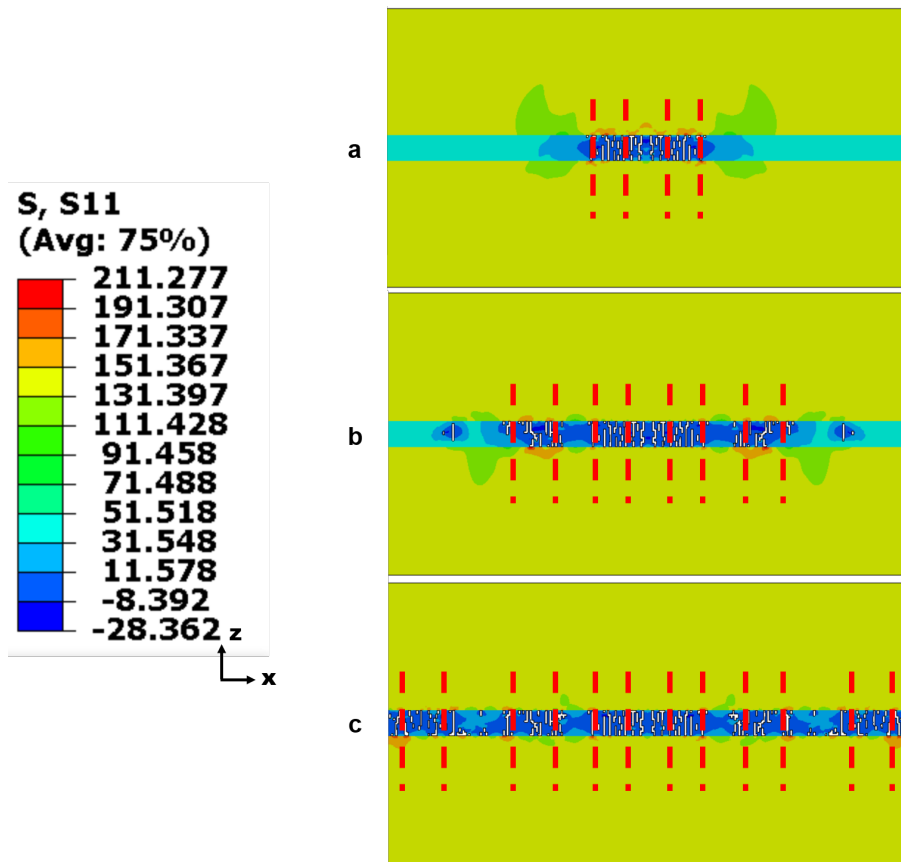


Figure 4.4. Cracks occurred in Model 1 with mesh size equal to 0.0075mm

The analysis of the stress-strain curve allows to confirm the mesh objectivity on the occurrence of the crack. Picture 4.5 shows the two curves plotted; in this case, they fit perfectly.

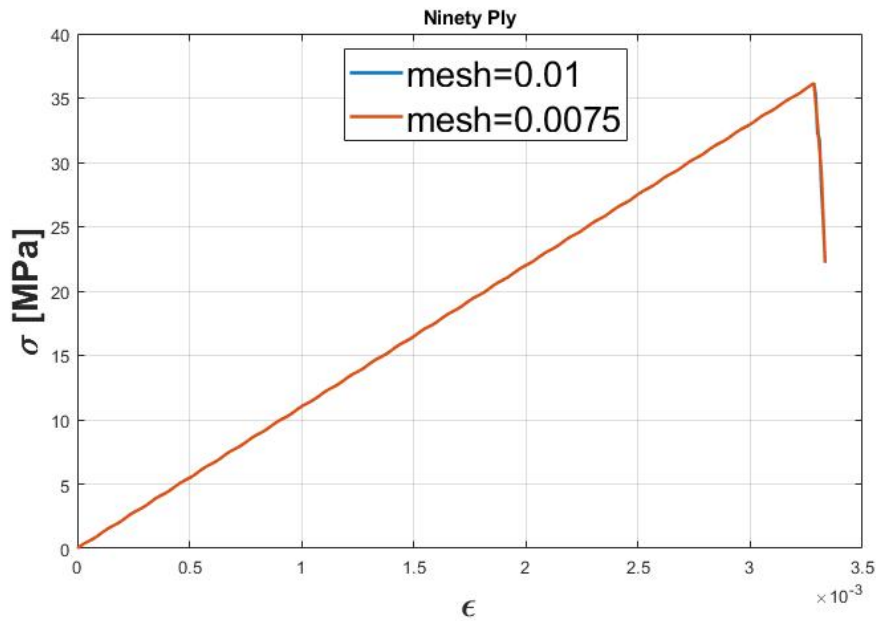


Figure 4.5. Stress-Strain curves of two mesh size of Model 1

4.1.2 Low Fidelity Model 2: transverse ply thickness 0.4mm

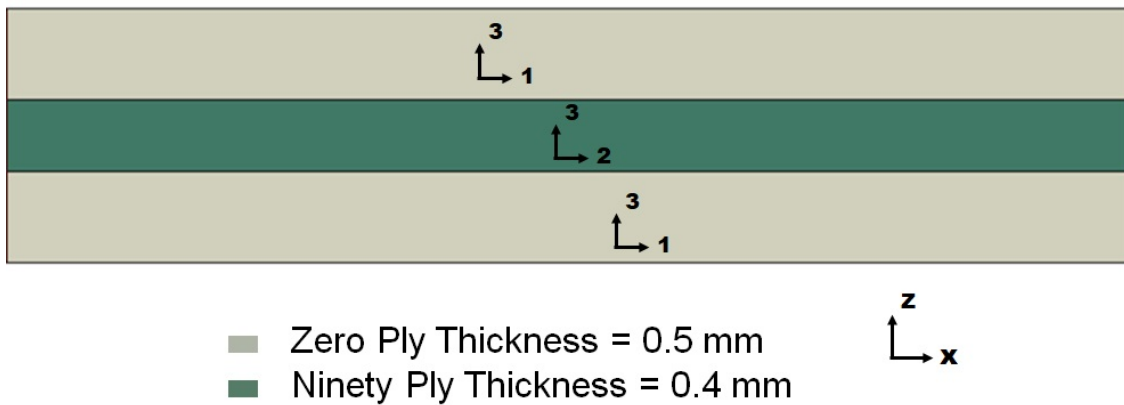


Figure 4.6. Low Fidelity Model 2

Model 2 has a transverse ply thickness of 0.4 mm: the paper of *Parvizi et Al.* [6] describes how the transition between thin and thick

ply occurs in this laminate, in fact all specimens with transverse ply thicker than this have a strain at the strength almost constant.

The strength of thick laminate can be linked to the strength of the unidirectional transverse ply with the equation found by *Laws and Dvorak*, as shown in section 1.3.

The first analysis is made with a mesh size analyzed is 0.035mm. This model uses solid elements C3D8, like Model 1. As explained before, cracks can be visualized as line spanning the entire ply or as a bunch of defects occurring at the same time.

Referring to picture 4.7, the first crack happens in the middle and then, more cracks take place at the average distance of 0.6mm from each other. The stress is plotted in the loading direction (x direction).

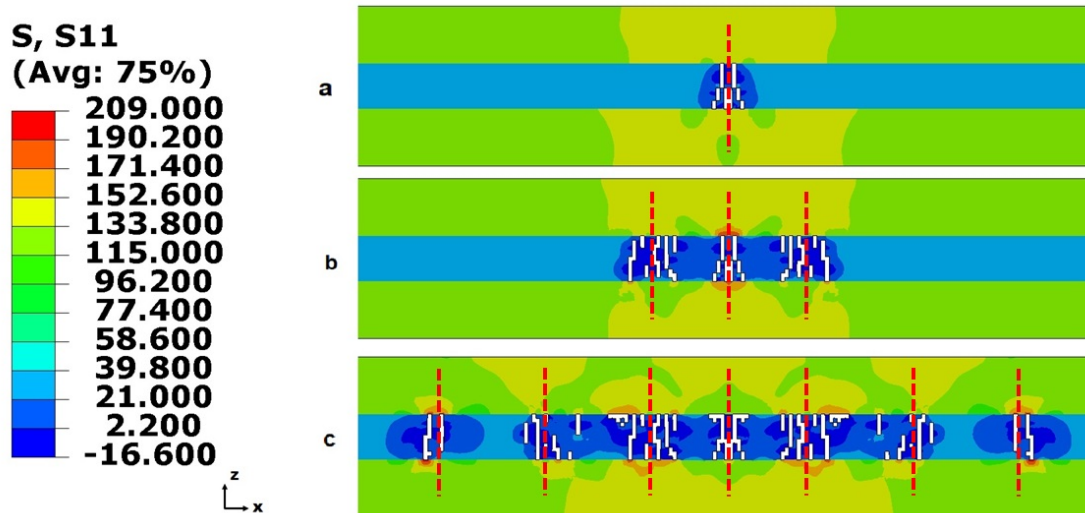


Figure 4.7. Cracks occurred in Model 2 with mesh size equal to 0.035mm

The second test of Model 2 has a mesh size of 0.025 mm. Cracks happens in the same spots as the previous test, as shown in picture 4.8. Here, more defects took place, due to numerical reasons, but the average cracking distance remains the same.

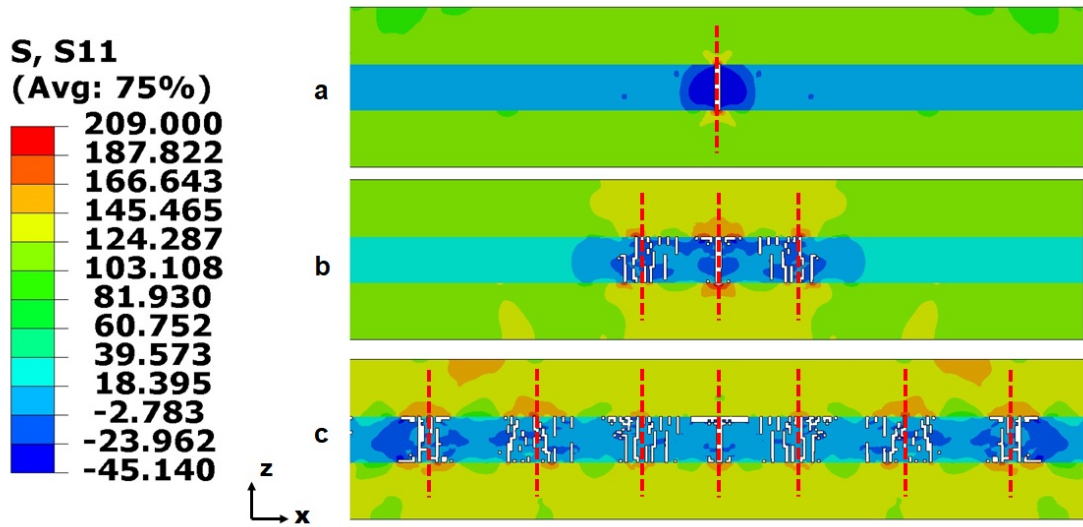


Figure 4.8. Cracks occurred in Model 2 with mesh size equal to 0.025mm

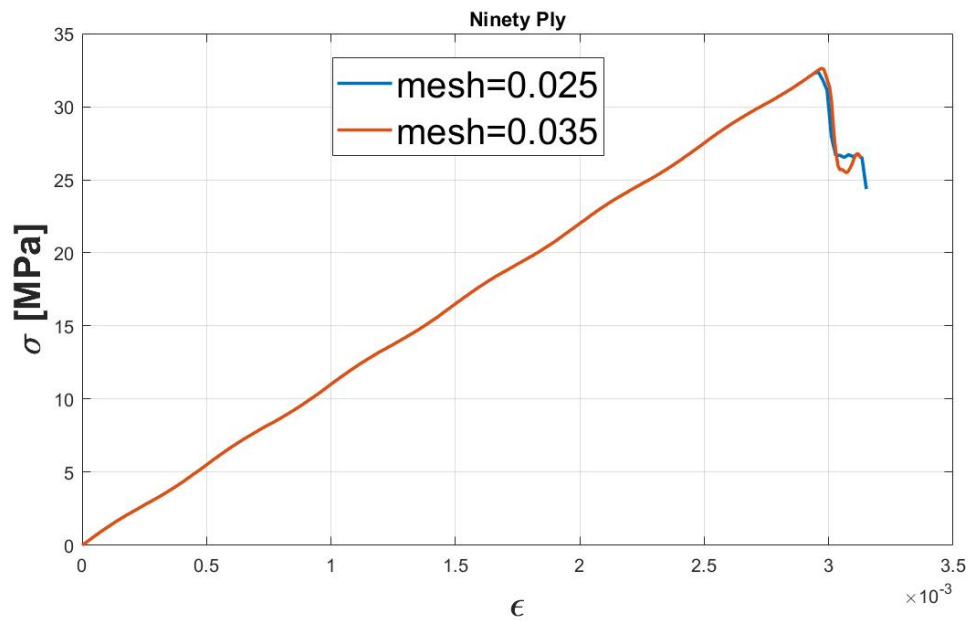


Figure 4.9. Stress-Strain curves of two mesh size of Model 2

The comparison between the Stress-Strain curves, reported in picture 4.9, shows some differences, due to more defects occurred in the test

with finer mesh.

4.1.3 Low Fidelity Model 3: transverse ply thickness 1mm

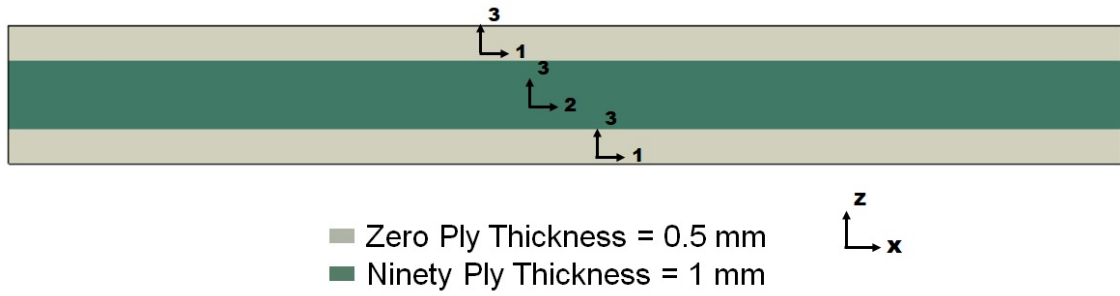


Figure 4.10. Model 3

Model 3, with a transverse ply thickness of 1mm, was analyzed with a mesh size of 0.08 mm and 0.06mm. Results are reported in pictures 4.11 and 4.12. These two models have a different sequence of cracking occurrence, but the crack spots and the average crack distance are the same. The shear lag distance for this model was found to be 1.1mm.

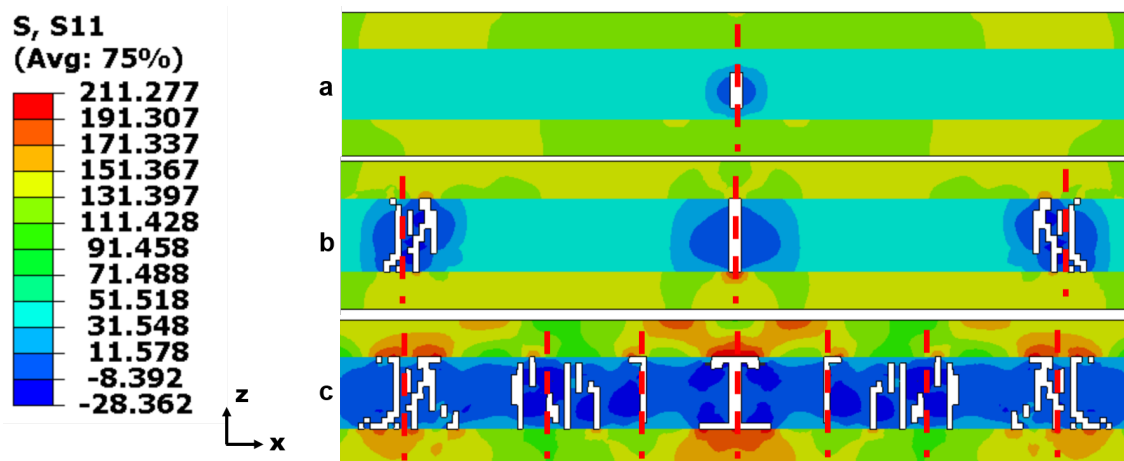


Figure 4.11. Cracks occurred in Model 3 with mesh size equal to 0.08mm

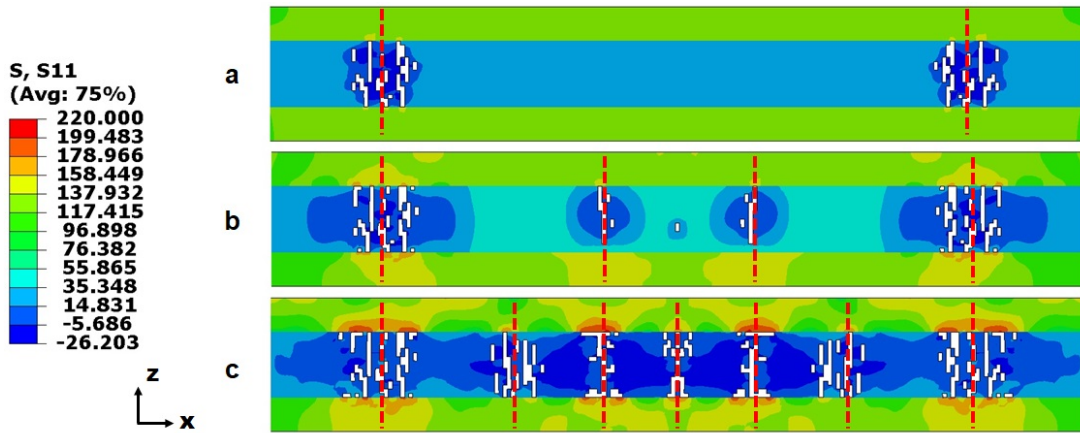


Figure 4.12. Cracks occurred in Model 3 with mesh size equal to 0.06mm

Due to the difference in cracking occurrence, the test with a bigger mesh size has a lower strength, which occurs at strain lower than the strain at the strength of the other test. The reason is that the crack in the middle takes place before any other cracks, but, after the occurrence of flaws at the sides, the two Stress-Strain curves fit almost perfectly.

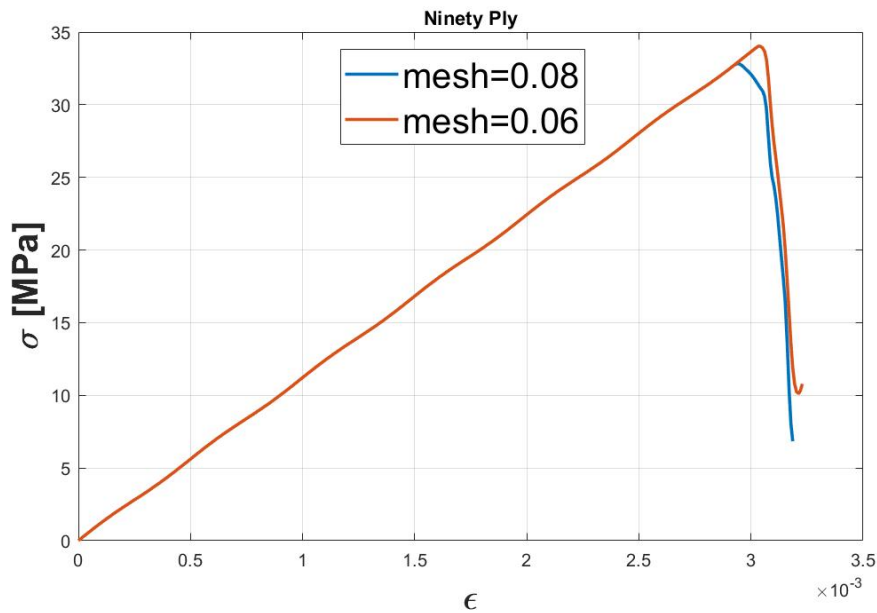


Figure 4.13. Stress-Strain curves of two mesh size of Model 3

4.1.4 Low Fidelity Model 4: thickest transverse ply (2d = 2 mm)

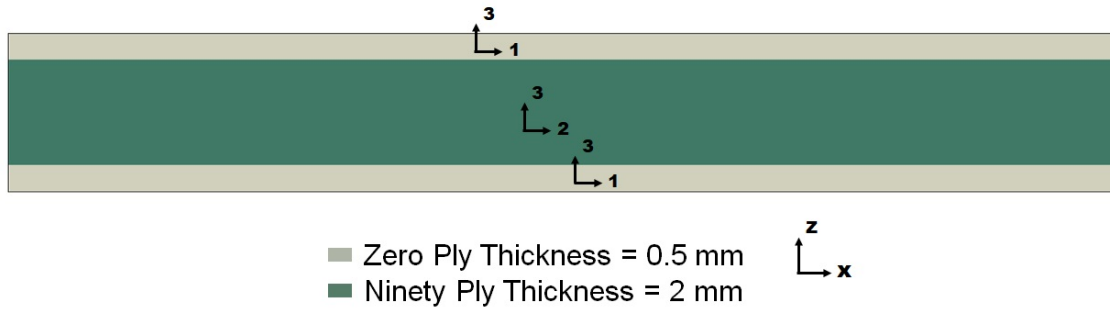


Figure 4.14. Low Fidelity Model 4

Model 4 is the one with the thickest transverse ply, equal to 2 mm. Here three cracks took place before the damage of the zero plies. As in the other models, two tests were performed, with mesh size 0.2mm and 0.1mm.

Both tests show an average cracking distance of 2.2 mm.

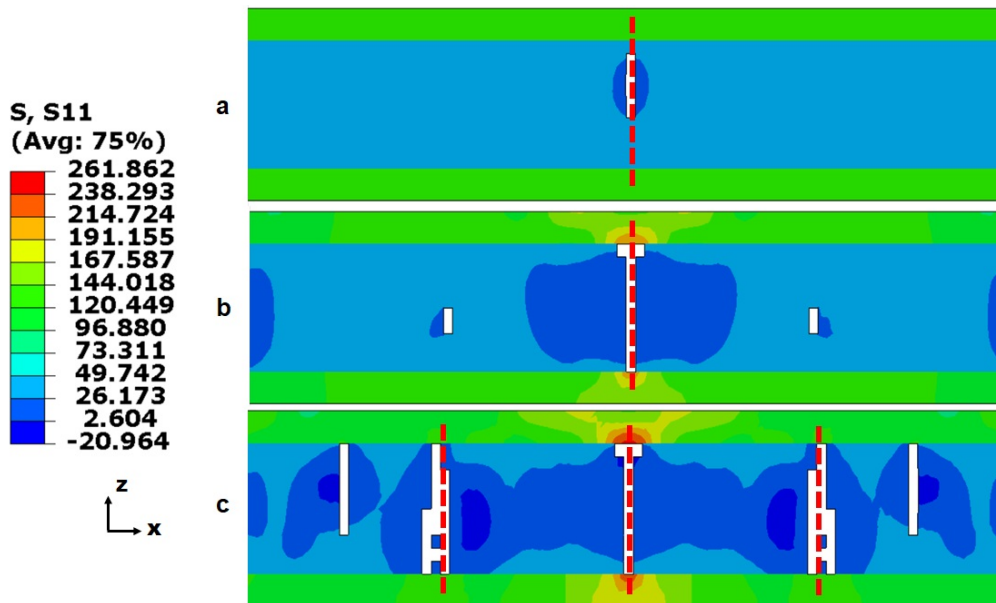


Figure 4.15. Cracks occurred in Model 4 with mesh size equal to 0.2mm

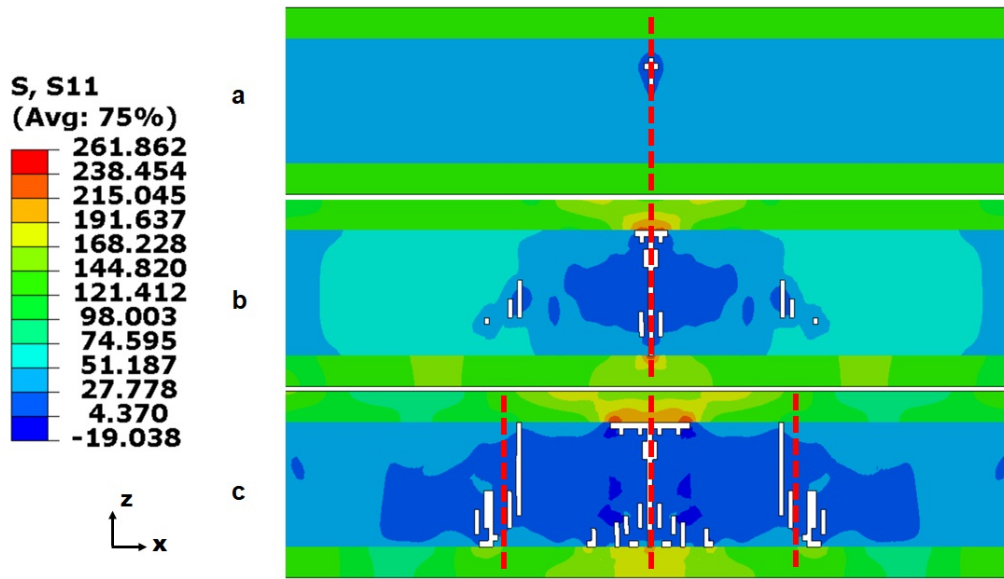


Figure 4.16. Cracks occurred in Model 4 with mesh size equal to 0.1mm

The cracking sequence was the same for both mesh sizes and the Stress-Strain curves fit very well.

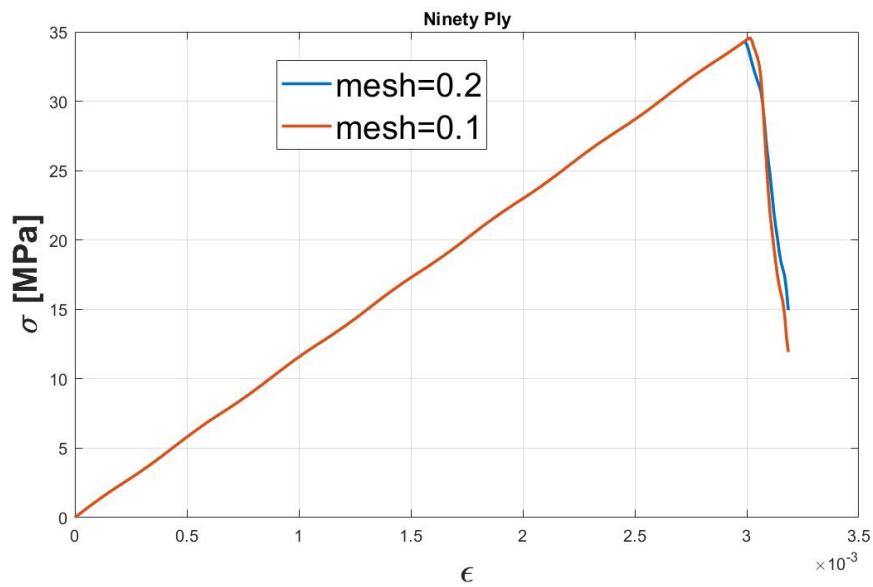


Figure 4.17. Stress-Strain curves of two mesh size of Model 4

4.1.5 Results of Low Fidelity Model

The Low Fidelity Model does not have enough information to extract reliable results in terms of strength, because the crack formation and propagation are affected by the random position of the fibers. However, the analysis of can give an idea of the behavior of the laminate: the stress-strain plot of the four models shows that the strain at the strength is higher in Model 1, while the other three have a similar value. This result agrees with the literature, but it still needs to be proved by the analysis of the High Fidelity Models.

In the next table, results of Low Fidelity Model are summarized. Once the RVE length is defined, it is possible to calculate the number of fibers contained in the transverse Ply of the High Fidelity Model.

Model	Ninety Ply Thickness	RVE Length	Number of Fibers	Strength	Strain at strength
MODEL 1	0.1 mm	0.2 mm	71	36.2 [MPa]	0.0033
MODEL 2	0.4 mm	0.6 mm	857	33 [MPa]	0.00297
MODEL 3	1 mm	1.1 mm	3930	34.1 [MPa]	0.00304
MODEL 4	2 mm	2.2mm	15720	34.5 [MPa]	0.0030

4.2 Onset of Microcracking

The onset of microcracking is considered to be the occurrence of the first defect in the model. According to the literature, this point coincides with the first drop of the Stress-Strain curve. The analysis aims at recording the strain at the strength and reproducing the behavior described first by *Parvizi et Al.* [6] (fig. 1.11).

4.2.1 High Fidelity Model 1

The RVE length of model 1 is 0.2 mm and takes into account 71 fibers. The model of the laminate is shown in picture 4.18:

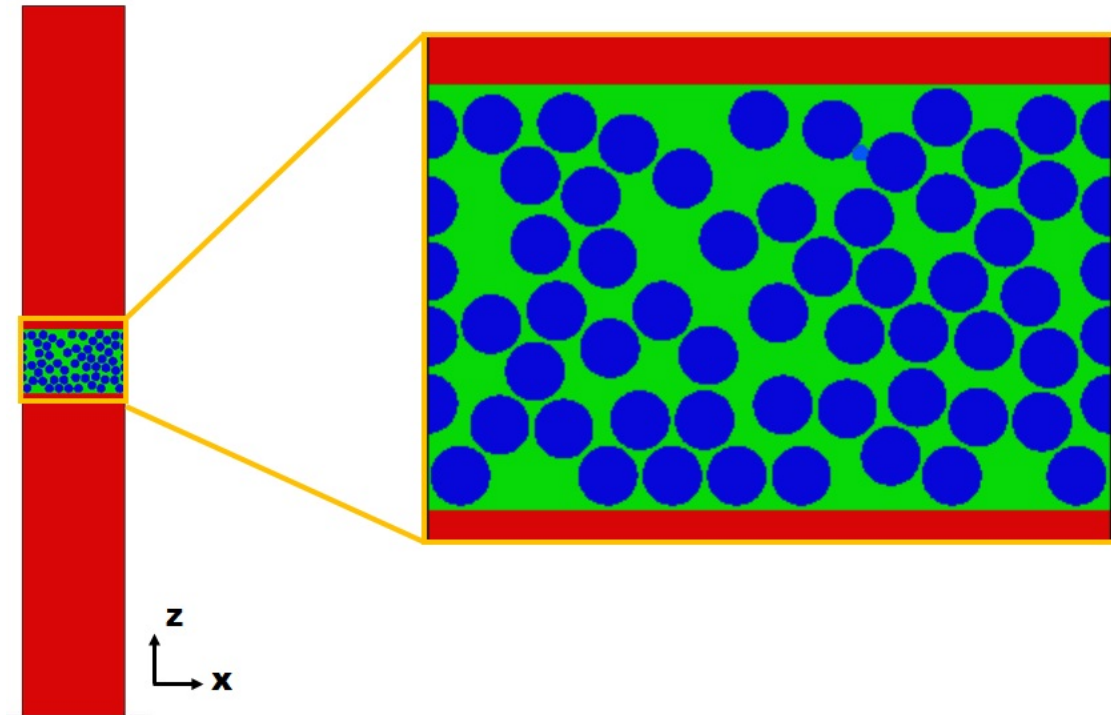


Figure 4.18. High Fidelity Model 1

In Model 1, the cracks start from three defects, which connect together forming a crack that spans the entire thickness. The initiation of the flaw occurs at the interface of the matrix and the fiber, where there is a stress concentration (fig. 4.19).

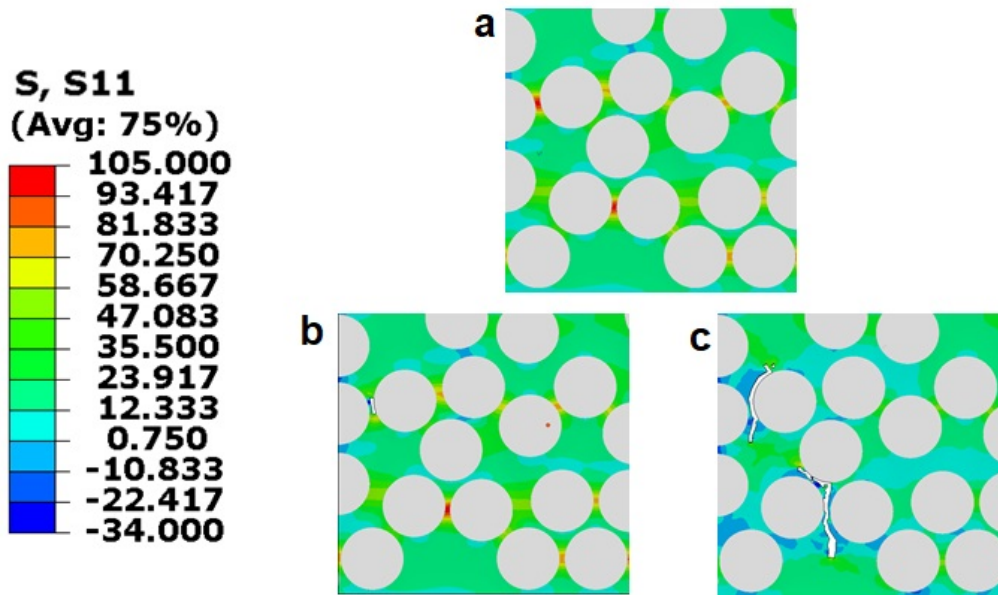


Figure 4.19. Crack formation at the fiber-matrix interface

Picture 4.20 shows formation of the cracks in sequence. The stress plotted is the stress in the loading direction σ_{11} , which is the x direction.

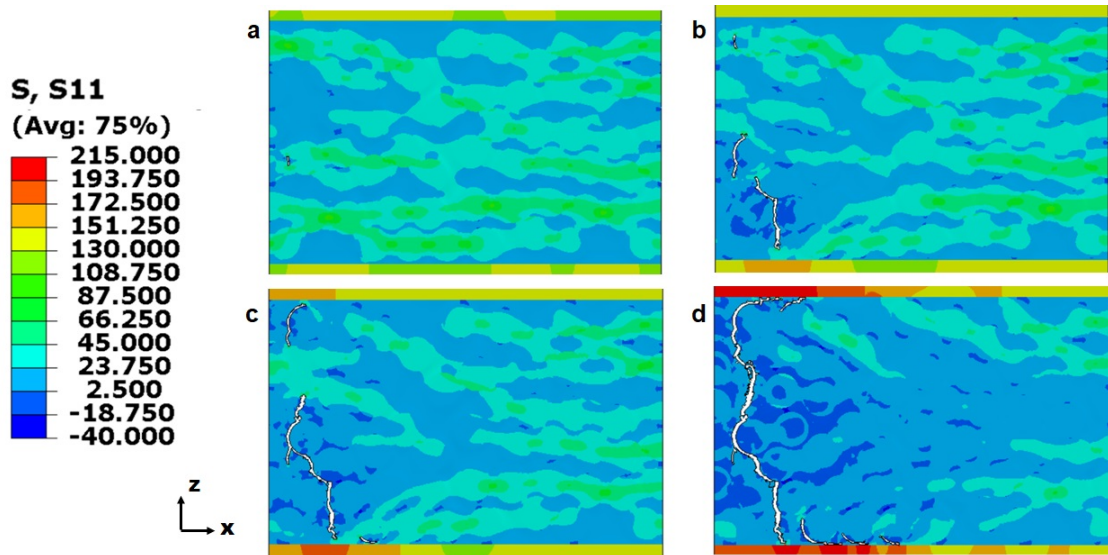


Figure 4.20. Crack formation and propagation through the thickness in Model 1

The Stress-Strain curve of the ninety ply has a main drop corresponding to the onset of the crack. From the plot, the strength and the respective strain can be found:

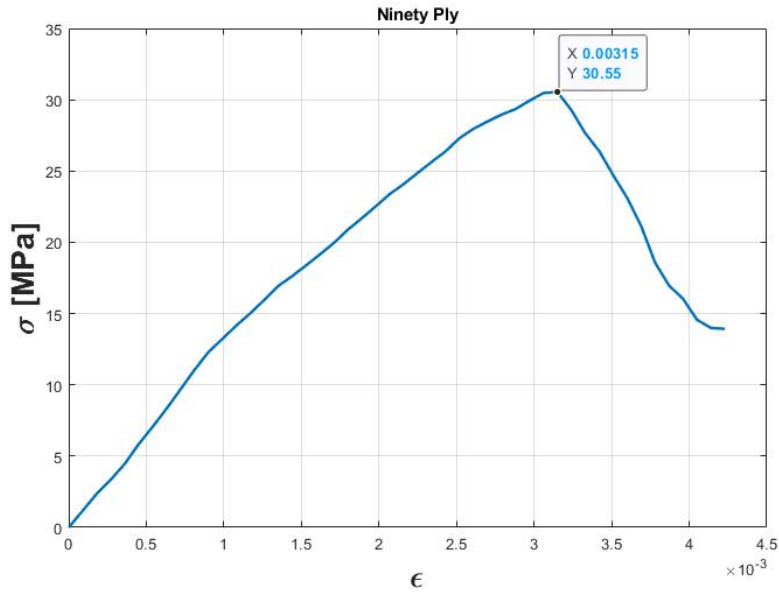


Figure 4.21. Stress-strain curve of the Model 1

Model	Ninety Ply Thickness	Strength	Strain at strength
MODEL 1	0.1 [mm]	30.55 [MPa]	0.00315

4.2.2 High Fidelity Model 2

The High Fidelity model has a length of 0.6 mm and 857 fibers have been placed in the transverse ply.

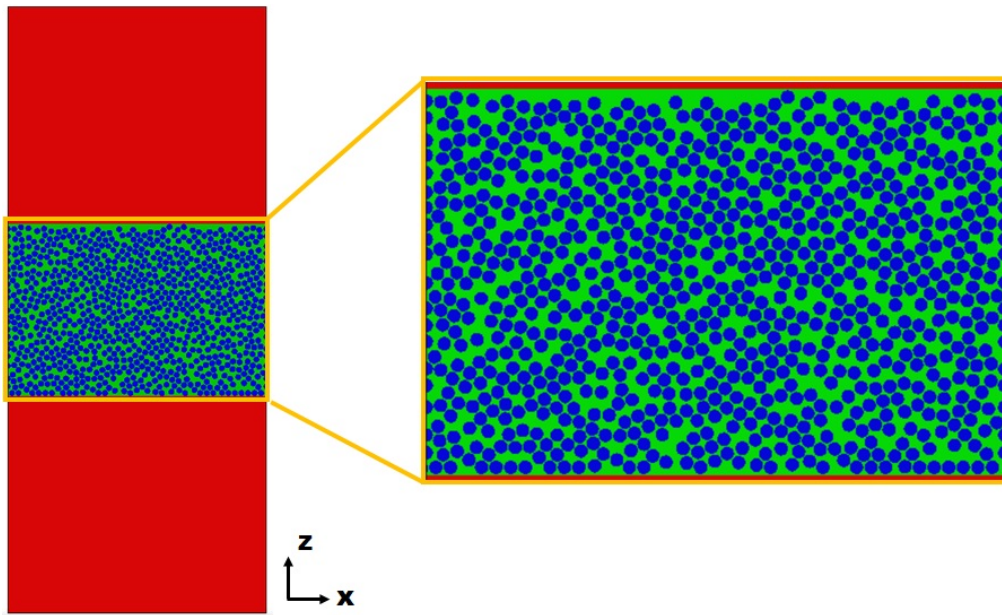


Figure 4.22. High Fidelity Model 2

Two defects occur at the same time: the flaw on the left starts in the middle of the ply at the interface between fibers and matrix, where there is a higher stress concentration (fig. 4.23).

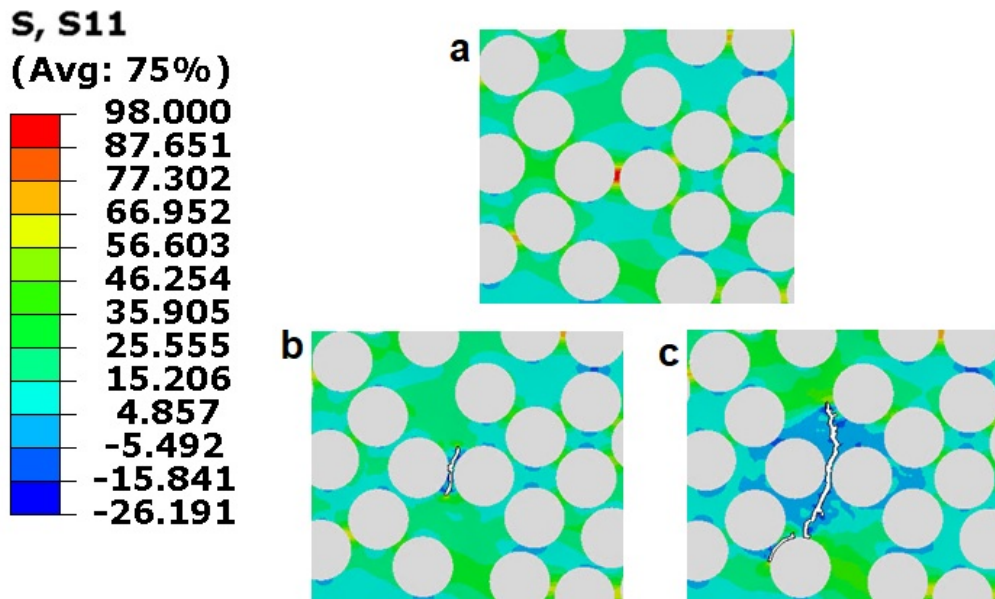


Figure 4.23. Crack formation at the fiber-matrix interface

The crack propagates through the thickness and, when it reaches the interface, small delamination takes place starting from the tip of the flaw. The presence of two cracks is not caused by an error in the RVE length, but the stress field is affected by the position of the fibers. Picture 4.24 shows formation of the cracks in sequence. The stress plotted is the stress in the loading direction, σ_{11} , which is the x direction.

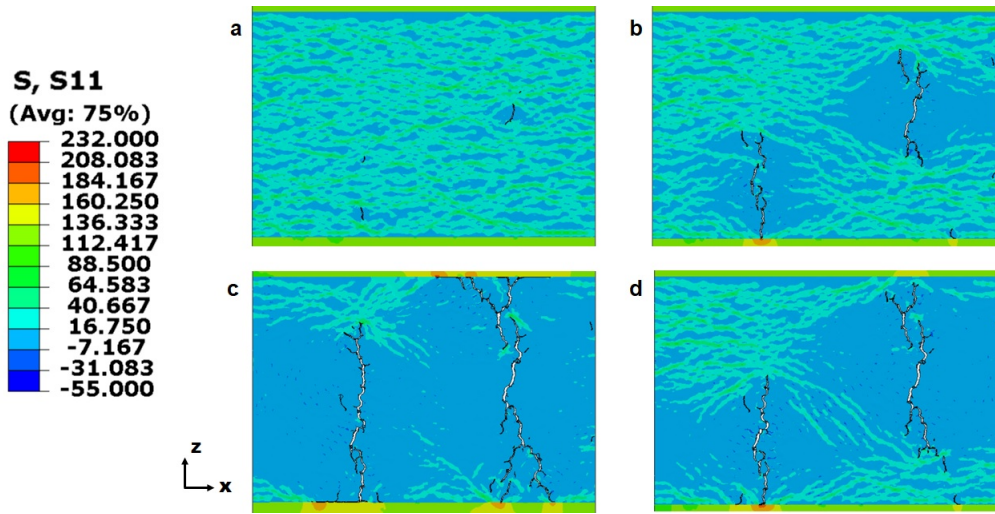


Figure 4.24. Crack formation and propagation through the thickness in Model 2

The stress-strain curve of the ninety ply has only one knee, corresponding to the onset of both cracks. The drop is very steep because two flaws are occurring simultaneously in the transverse ply.

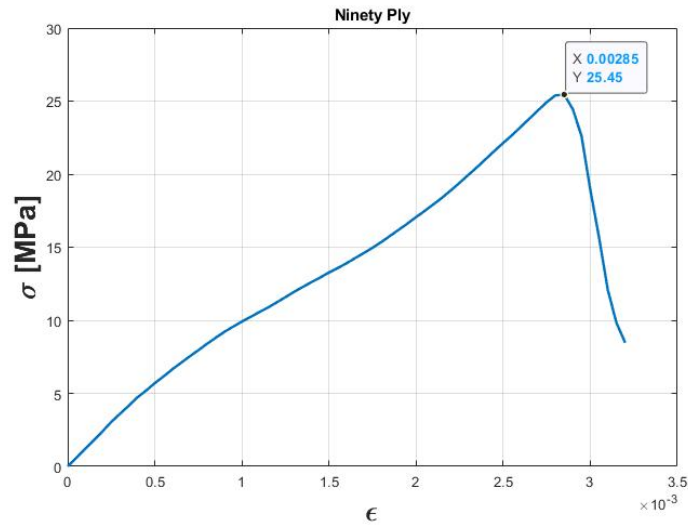


Figure 4.25. Stress-strain curve of Model 2

Model	Ninety Ply Thickness	Strength	Strain at strength
MODEL 2	0.4 [mm]	25.45 [MPa]	0.00285

4.2.3 Results of the onset of cracking

Figure 4.26 reports the mechanical strain corresponding to the onset of the microcracking phenomenon for both the Low Fidelity Model and the High Fidelity Model.

The Low Fidelity Model predicted a higher strain for both Model 1 and Model 2, with an error around 4% with respect to the critical value of the respective High Fidelity Model.

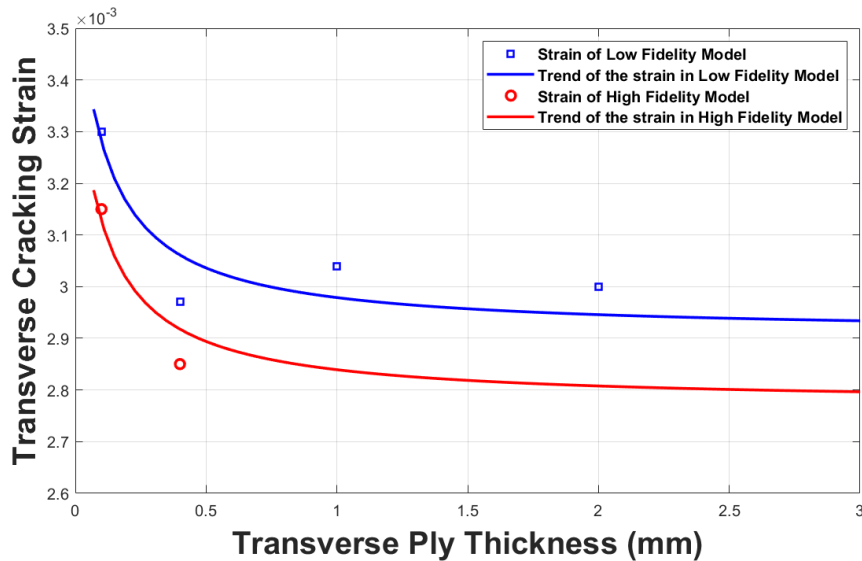


Figure 4.26.

The blue line represents the trend of the result in the low fidelity model; this trend is similar to the curve found by *Parvizi et Al.* [6]. It is possible to guess the trend of the results of the High Fidelity Models

(red line), considering the constant error between multi-scale models 1 and 2 and the respective Low Fidelity Model.

Chapter 5

Conclusions

This thesis studied the transverse cracking behavior of fiberglass reinforced epoxy laminates with finite element simulations. The purpose of the work was to predict the strength as well as the influence of transverse ply thickness on the onset of cracking.

The analyses were divided into two steps: first, a homogenized model of cross-ply laminates $[0/90_n]_s$ was built to determine the converged size of a Representative Volume Element (RVE) according to the shear lag theory.

Then, multi-scale RVEs, which accounts for fibers and matrix in the transverse ply, were modeled to find the onset of cracking and the transverse ply strength. The zero plies were modeled as homogenized material using Glass Fiber Reinforced Epoxy properties.

The failure was predicted using the Crack Band Model, proposed by *Bazant and Oh* [20]: in the homogenized model, the Hashin Criteria was applied to transverse and longitudinal plies. In the multi-scale model, the Maximum Principal Stress Criteria was used for the matrix and the Hashin Criteria for the zero plies. In this model, both matrix failure and fiber-matrix interface decohesion were taken into account.

The analysis of the homogenized models showed that the cracking distance increased with the increase of the transverse ply thickness. The length was always slightly greater than the ninety ply thickness.

Preliminary results on the strength and the strain at the strength were obtained by studying the stress-strain plot of the models: the laminate with the thinnest transverse ply had the highest strength,

while the other three models showed lower values.

The results of the detailed model showed that the onset of flaws started at the interface between fibers and matrix, where the stress concentration is high. Then, flaws grew and started connecting with each other, forming a dominant crack, which spans the entire transverse ply thickness. The fibers distribution affects the position and the path of the crack as well as the number of flaws.

The influence of the transverse ply thickness on the failure behavior of the *in situ* ply was confirmed according to the literature: the onset of cracks in the laminates with thinner transverse ply happened at a higher value of mechanical strain and strength.

Bibliography

- [1] N.Laws, G.J. Dvorak, *Progressive Transverse Cracking in Composite Laminates* J. of Composite Materials, 22 (1988)
- [2] K.W. Garrett, J.E. Bailey, *Multiple transverse fracture in 90 ° cross-ply laminates of a glass fibre-reinforced polyester*, J. of Material science 12 (1977), 157-168
- [3] A. Parvizi, J.E. Bailey, *On multiple Transverse Cracking in Glass Fibre Epoxy Cross-Ply Laminates*, J. of Material science 13 (1978), 2131-2136
- [4] G.T. Stevens, A.W. Lupton, *Some Factors Controlling Transverse Cracking in Cross-Ply Composites* J. of Materials science 12 (1977)
- [5] P.W.M. Peters, T.W. Chou, *Cross-ply cracking in glass and carbon fiber reinforced epoxy laminates*, Composites 18 (1987)
- [6] A. Parvizi, K.W. Garrett, J.E. Bailey, *Constrained cracking in glass fiber reinforced epoxy cross-ply laminate*, J. of Materials Science, 13 (1978), 195 - 201
- [7] L.G. Garcia, J. Justo, A. Simon, M. Mantic, *Experimental study of the size effect on transverse cracking in cross-ply laminates and comparison with the main theoretical models*, Mechanics of Materials 128 (2019), 24-37
- [8] D.L. Flaggs, M.H. Kural, *Experimental determination of In Situ Transverse Lamina Strength in Graphite/Epoxy Laminates*, J. of Composite Materials 16 (1982), 103-116
- [9] J.A. Nairn, *The strain Energy Release Rate of Composite Micro-cracking: A Variational Approach*, J. of Composite Materials, 23 (1989), 1106 - 1129
- [10] D.L. Flaggs, *Prediction of Tensile Matrix Failure in Composite Laminates*, J. of Composite Materials, 19 (1985),

- [11] J. Boniface et Al., *Transverse ply cracking in cross-ply CFRP laminates - initiation or propagation controlled?*, J. of Composite Materials, 31 (1997), 1080 - 1111
- [12] L.N.McCartney, *Recursive Method Of Calculation Stress Transfer in Multi-Ply Cross-Ply Laminates Subject to Biaxial Loading*, 1995
- [13] J.A. Nairn, *MAtrix Microcracking in Composites*, Comprehensive Composite Materials 2.13 (2000)
- [14] M. Herráez, D. Mora, F. Naya, C. S. Lopes, C. González, J. LLorca, *Transverse Cracking of Cross-Ply Laminate: a Computational Micromechanics Prospective* (2015)
- [15] L. Sun , J. Wang, H. Hu, A. Ni, *Simplified Computational Strategy Focused on Resin Damage to Study Matrix Cracking of The Cross-Ply Laminates Under Uniaxial Tension Load* (2019)
- [16] T.A. Sebaey, J. Costa, P. Miami, Y. Batista, N. Blanco, J.A. Mayugo, *Measurement of the In-Situ Transverse Tensile Strength of Composite Plies by Means of the Real Time Monitoring of Microcracking* (2014)
- [17] N.Laws, G.J. Dvorak, *Analysis of Progressive Transverse Cracking in Composite Laminates II. First Ply Failure* J. of Composite Materials, 21 (1987)
- [18] P.A.Carraro, E. Novello, M. Quaresimin, M. Zappalorto, *Delamination onset in symmetric cross-ply laminates under static loads: Theory, numerics and experiments* , Composite Structures 176 (2017), 420-432
- [19] Z. Hashin, *Failure Criteria For Unidirectional Fiber Composites* J. of Applied Mechanics, 47 (1980), 329-334
- [20] Z. Bazant, B.H. Oh, *Crack Band theory for fracture of concrete* Material and Structure 16 (1983)
- [21] M. Jirasek, Z.P. Bazant, *Inelastic analysis of structures*, John Wiley & Sons, London and New York (2002)
- [22] H.L. Cox, *The Elastic and the Strength of paper and other fibrous materials*, British Journal of applied Physics 3 (1952), 72-79
- [23] M. Maiarù, *Effect of uncertainty in matrix fracture properties on the transverse strength of fiber reinforced polymer matrix composites* 2018

- [24] M.W. Hyer, *Stress Analysis of Fiber-Reinforced Composite Materials*, WCB McGraw-Hill, 1988
- [25] R.M Jones, *Mechanics of Composite Materials*, McGraw-Hill, 1999.
- [26] R.F. Gibson, *Principle of Composite material Mechanics*, McGraw-Hill, 1994
- [27] T.W. Clyne, D. Hull, *Composite Materials - Third edition*, Cambridge University Press, 2019
- [28] Alan Hiken, *The Evolution of the Composite Fuselage: A Manufacturing Perspective*, 2018